**Universidade de Aveiro**
**2022**

**Daniel Marques Gadelho**

# Desenvolvimento de protótipo para recuperação de energia das ondas

Development of a prototype for wave energy recovery

**Universidade de Aveiro**
**2022**

**Daniel Marques Gadelho**

# Desenvolvimento de protótipo para recuperação de energia das ondas

## Development of a prototype for wave energy recovery

Trabalho de projeto apresentado à Universidade de Aveiro para cumprimento dos requisitos necessários à obtenção do grau de Mestre em Engenharia de Automação Industrial, realizada sob a orientação científica do Doutor Jorge Augusto Fernandes Ferreira, Professor Associado do Departamento de Engenharia Mecânica da Universidade de Aveiro, e do Doutor António Manuel de Amaral Monteiro Ramos, Professor Auxiliar do Departamento de Engenharia Mecânica da Universidade de Aveiro.

- UID/EMS/00481/2019-FCT – FCT – Fundação para a Ciência e a Tecnologia; e CENTRO-01-0145-FEDER-022083 – Programa Operacional Regional do Centro (Centro2020), através do Portugal 2020 e do Fundo Europeu de Desenvolvimento Regional

**o júri**

presidente

Prof. Doutor Marco Paulo Soares dos Santos
professor auxiliar da Universidade de Aveiro

vogais

Prof. Doutor Daniel Gil Afonso
professor adjunto da Escola Superior de Design, Gestão e Tecnologias da Produção de Aveiro-Norte

Prof. Doutor Jorge Augusto Fernandes Ferreira
professor associado da Universidade de Aveiro

**agradecimentos**

Quero agradecer ao Prof. Doutor Jorge Augusto Fernandes Ferreira e ao Prof. Doutor António Manuel de Amaral Monteiro Ramos pela orientação e pelas opiniões que foram dando ao longo deste trabalho, ao Eng. Rui Pedro Vieira Heitor pelo apoio à execução de trabalhos laboratoriais, ao Eng. António José da Fonseca Festas pela maquinação de algumas das peças necessárias para o desenvolvimento deste trabalho, ao meu colega Gonçalo Pires pelo apoio e acompanhamento neste trabalho e aos meus familiares, amigos e restantes colegas que me acompanharam ao longo dos meus estudos.

**palavras-chave** Energia Renovável, Conversor de Energia das Ondas, Conversor de Energia.

**resumo**

Atualmente, estimativas apontam que o consumo de eletricidade crescerá na Europa e a nível mundial de forma bastante significativa. Esta procura por energia elétrica não pode ser suportada por combustíveis fósseis, o que levou a União Europeia a estabelecer como objetivo a redução das fontes tradicionais de energia não-renovável. O fornecimento de energia deve ser tendencialmente suportado por fontes renováveis. O vento e o sol estão entre as fontes de energia renovável mais significativas. As tecnologias de conversão da energia dos oceanos ainda se encontram em fase de desenvolvimento, teste e validação experimental, tendo alguns desses dispositivos fracassado dadas as adversidades do meio onde operam, que é o mar. Estas tecnologias incorporam, na sua grande maioria, sistemas mecânicos complexos, em que tem contacto direto de mecanismos com movimentos relativos com o mar, e têm tido como resultado a reduzida produção de energia e o reduzido tempo de vida em operação. Neste projeto apresenta-se o desenvolvimento da componente elétrica de um dispositivo, cujo conceito tem vindo a ser desenvolvido, para um mecanismo Power Take Off (PTO) para a recuperação da energia das ondas do mar.

**keywords** Renewable Energy Sources, Wave Energy Converter, Power Take-Off.

**abstract**

Currently, estimates indicate that electricity consumption will grow significantly in Europe and worldwide. This demand for electricity cannot be supported by fossil fuels, which led the European Union to set a goal of reducing traditional sources of non-renewable energy. The energy supply should tend to be supported by renewable sources. Wind and sun are among the most significant renewable energy sources. Ocean energy conversion technologies are still in the development, testing and experimental validation phase, with some of these devices having failed given the adversities of the environment in which they operate, which is the sea. These technologies incorporate, for the most part, complex mechanical systems, in which there is direct contact of the mechanisms with relative movements with the sea, and have resulted in reduced energy production and reduced operating life. This project presents the development of the electrical component of a device, whose concept has been developed, for a Power Take Off (PTO) mechanism, for the recovery of energy from sea waves.

# Table of Contents

# List of Figures

# List of Graphs

# Acronyms

| | |
|---|---|
| **DFIG** | Doubly-Fed Induction Generator |
| **EU** | European Union |
| **HPA** | Heaving Point Absorber |
| **HVDC** | High Voltage Direct Current |
| **IEA** | International Energy Agency |
| **OPA** | Oscillating Pitch Absorber |
| **OWC** | Oscillating Water Column |
| **OWSC** | Oscillating Wave Surge Converter |
| **PTO** | Power Take-Off |
| **RES** | Renewable Energy Source |
| **RPM** | Rotation per Minute |
| **SCIG** | Squirrel Cage Induction Generator |
| **VFD** | Variable-Frequency Drive |
| **WEC** | Wave Energy Converter |

# 1. Introduction and Objectives

## 1.1. Introduction

According to the International Energy Agency (IEA), in a report released, it is expected that by 2040, energy consumption worldwide will increase by more than 50%, and by 2050 energy consumption in Europe will double [1]. This brings environmental impacts due to the use of electric energy sources by fossil fuels, in which, more than 75% of the European Union's greenhouse gas emissions come from the energy sector [2]. That's why the European Union (EU) intends to set a goal of reducing traditional sources of non-renewable energy by between 80 and 95% by 2050 [3].

At the moment, we have mainly wind and sun as renewable energy sources. We also have the sea, which is still under development, and some of these technologies have failed due to the environment in which they are found. But the problem with using a grid with 100% renewable energy sources is its intermittence, for example, we don't have wind every day, and the sun is only present during the day, and, with the use of electric cars, with the practicality of charging them in each one's own homes during the night, the nocturnal consumption (during the dawn) that before could be insignificant, will become very significant.

To mitigate this type of problem, the solution will be the use of a hybrid and intelligent network. In these networks, energy comes from various types of energy sources and implies the existence of large-scale batteries to counteract the intermittence of some renewable sources [4] [5].

Wave energy is the most consistent of renewable energy sources as waves remain throughout the day, even if they change in power and size, which are easily predictable by meteorological movements [6].

In this dissertation, one of the purposes of this work is to continue the development of concepts in support of two other master's dissertations [7] [8]. In these previous works, a new concept for a Power Take-Off (PTO) mechanism has been developed for the recovery of wave energy, in which it has already been developed:

- the mechanical design of the linear motion to rotary motion conversion system;
- the coupling system to a three-phase generator;
- and the geometry of the buoy to be used in the PTO.

## 1.2. Objectives

With this work, it is intended to continue to develop a prototype for the recovery of potential energy from waves, developing the electrical component of the device. The concept to be explored is based on a mobile mass (buoy) that moves vertically in relation to a fixed floating structure in such a way that it makes possible the reduction of mechanical couplings in contact with water and simplifies the mooring systems.

In this project work, the prototype of the system will be built and some tests will be carried out in the laboratory, in order to characterize the prototype, namely in terms of efficiency in energy conversion.

Intentionally blank page.

# 2. State of Art

## 2.1. Types of Getting Energy from the Ocean

There are several ways of obtaining energy in the ocean, in which, in relation to renewable energies, there are the following possibilities:

- The wave energy, which is a type of renewable energy where sea waves originate from the action of the wind on the sea surface [9];
- The tidal energy that derives from the kinetic or potential energy of the water that reach a lower or higher altitude, where the greater the tidal amplitude, the greater the amount of energy that can be produced [10];
- The geothermal energy of the seas, which is obtained through the difference in temperature between the warmest layer at the surface and the coldest layer at the bottom of the ocean however these systems require a large diameter pipe to pump water to the surface and several heat exchange cycles are required to generate electricity [11];
- The thermal energy of the oceans obtained through a plant that produces fresh water, destined to vaporize the salt water in which the steam, in turn, drives the turbines to generate energy [12];
- The osmotic energy which is associated with the salinity gradient and which consists of the entropy difference between the two types of water, separated by semipermeable membranes for the migration of salt ions by osmosis, thus creating a low power current [13];
- And the hydro energy that is located in the rivers, where the movement of the riverbed is stopped and accumulated in order to concentrate potential energy and when the mass of water is released, it passes through a turbine in kinetic energy, generating energy and then the process is interrupted until there is enough water for the next flush [14].

*Figure 1 - Wave energy [15]*

*Figure 2 - Tidal energy [16]*

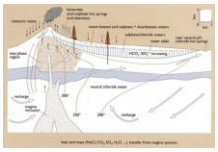

*Figure 3 - Geothermal energy of the seas [17]*

*Figure 4 - Thermal energy of the oceans [12]*

*Figure 5 - Osmotic energy [18]*

*Figure 6 - Hydro energy [19]*

## 2.2. Systems Classification

Wave Energy Converter (WEC) systems can be classified by their point of application, depth and distance from shore, PTO and type of mooring.

### 2.2.1. Point of Application

Depending on the point of application, WEC systems can be divided into (Figure 7):

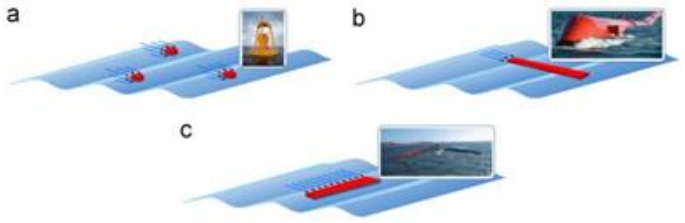


*Figure 7 - WEC systems classification [20]*

- Point absorbers (a), which are devices that have small dimensions in relation to the incident wavelength where this can be a floating structure that rises and falls on the surface of the water or a submerged structure, depending on the pressure differential, which, given their small size, the wave direction is not important for these devices and these can be subdivided into two subcategories in relation to the movement: those with a translational movement or those with a rotational movement of the buoy;
- Attenuators (b) that are parallel to the predominance of the navigation wave and climb the waves;
- And terminators (c) that have their main axis parallel to the wavefront (perpendicular to the prevailing wave direction) and physically intercept the waves [20].

### 2.2.2. Depth and Distance to Shore

WEC systems can be categorized according to distance from shore or depth in relation to the sea line, as we can see in Figure 8.

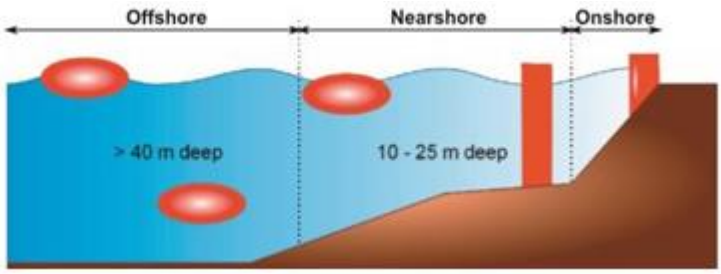


*Figure 8 - Offshore, nearshore and onshore [20]*

In terms of depth, onshore systems can reach a depth of 10 meters, while nearshore systems have depths between 10 and 25 meters, while offshore systems are at least 40 meters deep.

In terms of the distance from the coast, onshore systems have a distance of less than 10 meters, while nearshore systems have a distance between 10 and 20 meters, then there are intermediate systems with a distance between 20 and 50 meters, and finally, offshore systems with a distance greater than 50 meters.

Regarding the advantages and disadvantages of each system, the onshore systems have the advantage of being located close to the distribution network, having an ease of maintenance, having a less robust construction and having a less expensive manufacture. Their disadvantages are the fact that they are influenced by the tides, mass production is prohibited due to the laws of conservation of the coast and nature, and due to its location, the waves are of low energy density giving low power.

On the other hand, the offshore systems have the advantage that, due to their location, the waves have a high energy density, giving great power, while their disadvantages are the fact that they require great robustness, are more expensive and have complex maintenance [20].

### 2.2.3. Power Take Off (PTO)

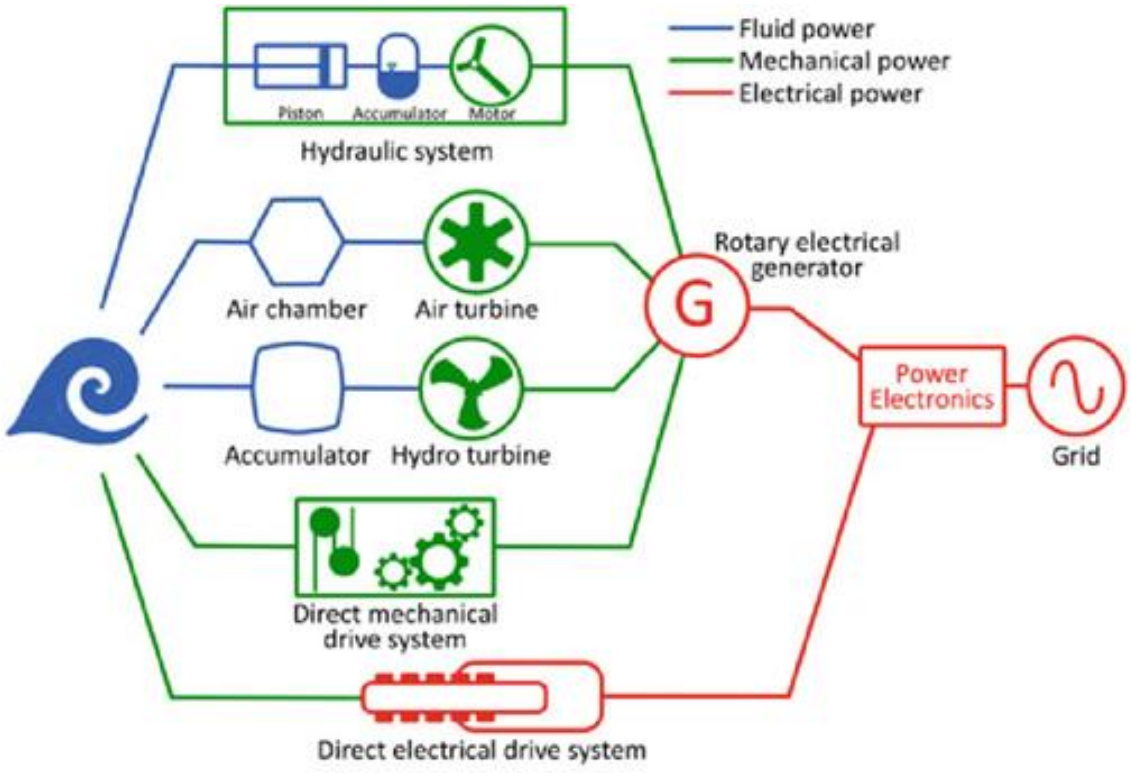


*Figure 9 - Power Take Off (PTO) [21]*

The PTO (Figure 9) is the WEC subsystem responsible for transforming the kinetic and potential energy of sea waves into electrical energy. Initially turbines were developed, followed by pneumatic and hydraulic cylinders and more recently linear generators. Other forms of conversion are currently being studied, namely the use of two sets of PTOs simultaneously, as is the case of linear generators with a hydraulic circuit.

### 2.2.4. Mooring

The mooring has the purpose of fixing the WEC system to a geographic point in order to remove greater powers through inherent forces in the waves of the sea, preventing unwanted movements of the structure.

There are different types of anchors for different types of technologies (Figure 10).

The lashings can be chains, synthetic yarn ropes with gravity anchors, built-in drag, driven suction, vertical load, drilled and towed [22] [23].


*Figure 10 - Mooring in conventional system and TAUT-LEG system [22]*

- **Scattered Moorings**

Catenary moorings are high-precision, suspended lines that reach the seabed horizontally, so that the anchor point is subjected only to horizontal forces. Restoration forces are generated mainly by the weight of the anchor lines enabling a static equilibrium.

Multi-channel mooring consists of high-precision lines that incorporate weights and buoys to form S-type or Wave-type configurations.

Spread mooring consists of low-precision lines with the anchor point capable of resisting horizontal and vertical forces. Restorative forces are generated primarily by the elasticity of the mooring line. The mooring lines of a Taut Leg are orthogonal to the sea floor, with the restorative force generated primarily by the change in buoyancy of the upper structure.

- **Single Point Moorings**

Tower mooring consists of a low-precision internal or external catenary anchor attached to a floating structure, allowing for paint-proofing adverse situations around the tower.

Low Catenary Anchor Leg Mooring (CALM) consists of a high precision floating structure that is anchored to an anchored catenary buoy and is capable of forming a weathervane around the anchored buoy.

The High Single Anchor Leg Mooring (SALM) consists of a high precision floating structure and is anchored to a single buoy.

The Elevated Articulated Loading Column (ALC) consists of a floating structure moored with a weathervane around a hinged column at the bottom, which has a swiveling motion above the waterline.

Single Point Mooring and Reservoir (SPAR) allows storage of a fluid (oil or hydrogen) for attachment and a floating structure upwind around an anchor point.

Fixed tower mooring consists of an anchor on the seabed that allows the moored floating structure to reach the weather vane around the anchor point.

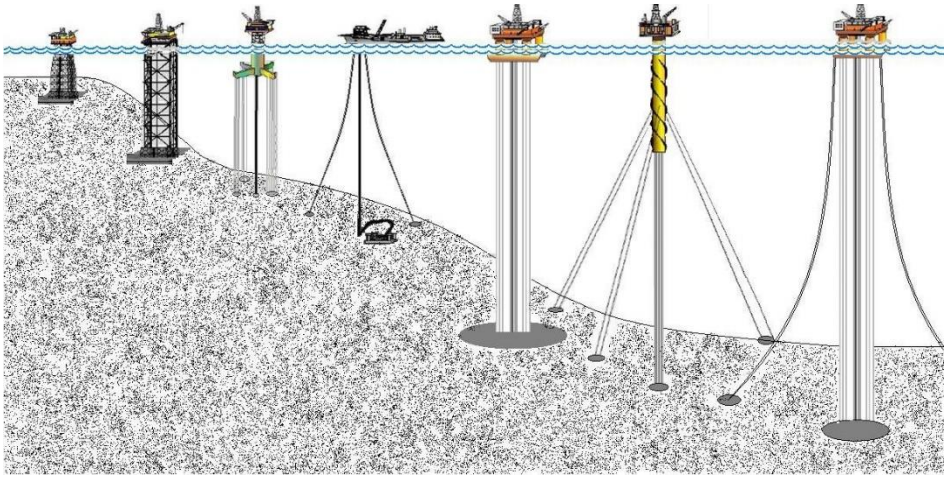

*Figure 11 - All modern mooring systems [20]*

- **Dynamic Moorings**

Active mooring is a low-precision technique that consists of spread fixing around the floating structure, where the inner end of each fixing line is held by a controlled winch. A central computer controls the tension of the anchor lines to maintain a fixed position on the seafloor.

Propulsion is a low-precision technique that consists of positioning a floating structure above a fixed point on the seabed using thrusters that are controlled from a central computer.

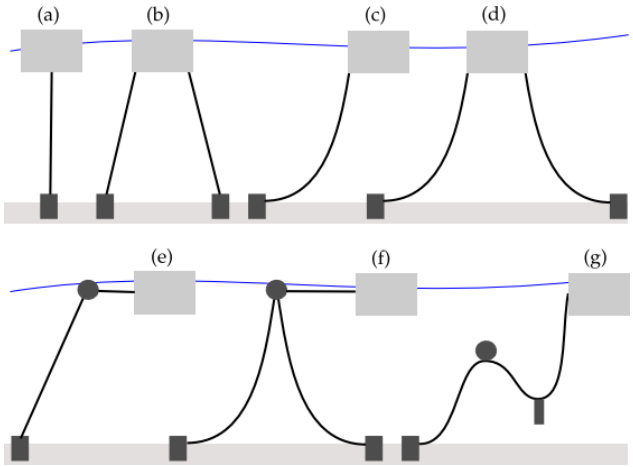


*Figure 12 - Mooring in WEC systems [24]*

In Figure 12 it is possible to compare the different anchoring processes in wave energy conversion systems: (a) Taut, (b) Taut Spread, (c) Catenary, (d) Multi-Catenary, (e) SALM, (f) CALM and (g) Lazy-s.

## 2.3. Types of WEC Devices

WEC systems are divided into 3 categories based on the point of application, namely terminators (section 2.3.1, 2.3.2 and 2.3.3), point absorbers (section 2.3.4 and 2.3.5) and attenuators (section 2.3.6). There is also the existence of prototypes in the investigation phase inserted in several PTO categories (section 2.3.7).

### 2.3.1. Terminators – Oscillating Water Column (OWC)

The OWC was one of the first technologies to be developed. The OWC is based on the energy of the oscillation caused by the waves of the sea inside an air chamber, able to admit the reversible movements of the tide. This cyclic flow generates motion in the turbine.

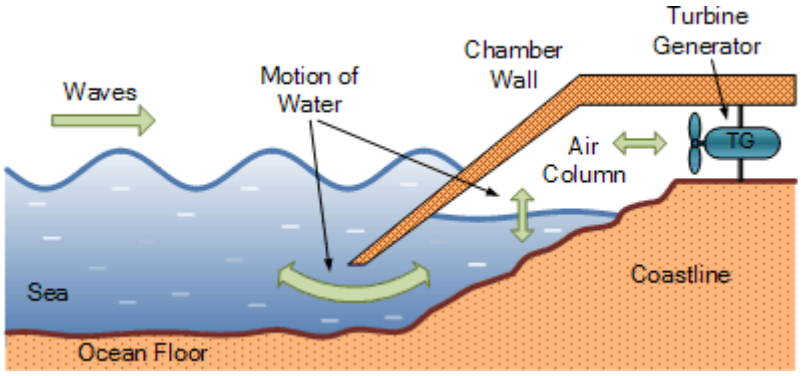


*Figure 13 - PICO Power Plant [25]*

We have, as an example, the PICO Power Plant developed by Aquaret®, on the coast of the island of Pico in the Azores archipelago. This company was a pioneer in the electrical distribution network. It uses a hollow structure made of concrete and steel, partially submerged, with two openings. The lower part of the structure is in contact with the sea and the upper part with the atmosphere. When the wave enters the structure, it pressurizes the air contained within it, forcing it to exit through a duct, where a turbine is mounted that converts the displacement of the vertical air mass into angular velocity. When the wave retreats, it drags the air mass again, creating a reversible movement in the turbine, that is, the turbine admits movements in both directions [25]. The kinetic energy in the turbine blades drives the induction generator, converting it into electrical energy.

Considering the disadvantages of this type of technology, namely the low energy level of the wave movement on the coast and the erosion problems (due to the sediments transported by the waves), floating systems were developed. This type of technology is observed in the OSPREY [26] being a nearshore wreck structure (in shallow waters) with a mooring system. There is also a technology, but not moored as is the case of the Might Whale [27] which has the same characteristics, but maintenance is more difficult and energy transport costs are higher.

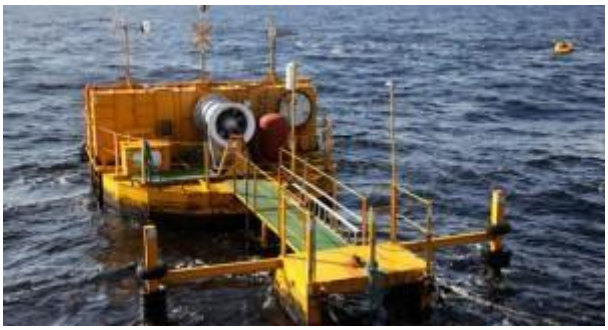

Figure 14 - OSPREY [26]

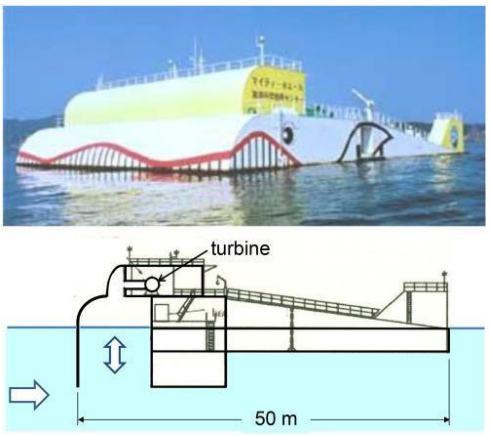


Figure 15 - Might Whale [27]

In offshore, we can mention the MRC 1000 [28] from Orecon® which, unlike the Osprey and Might Whale, is fixed to the ground with a single mooring point and with a greater number of turbines, increasing energy efficiency.

Figure 16 - MRC 1000 [28]

Finally, the Tunneled WEC technology [29] works with a multi-resonant oscillating water column (MOWC). SeWave®, in cooperation with Wavegen®, developed a new approach to onshore OWCs, based on the detonation of several tunnels in a cliff, linked together to form a column of water. The PTO will consist of a standard air turbine system. While there are significant complications during blasting, the company believes that the project represents a viable method of implementation in the Faroe Islands given the coastal characteristics.

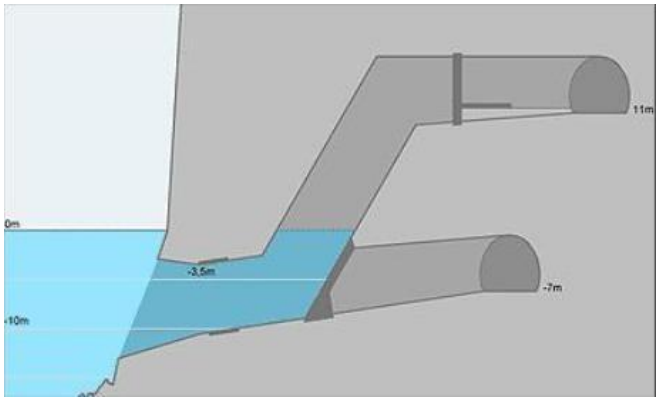


Figure 17 - Tunneled WEC [29]

### 2.3.2. Terminators – Oscillating Wave Surge Converter (OWSC)

In the class of OWSC, Aquaret® has developed the WAVEROLLER [30]. This technology consists of the use of an articulation plate, fixed to the seabed, at depths of up to 20 meters and oriented perpendicularly in the direction of wave propagation, oscillating like a pendulum, but inverted due to the movement of water particles. The kinetic energy created in the pistons coupled to the joint is transformed into electrical energy through a generator. There is an example of this technology installed in Peniche (Portugal) 900 meters from the coast, consisting of three units of 100 kW each, connected to the electricity grid.

*Figure 18 - WAVEROLLER [30]*

For larger waves, the company Aquamarinepower® developed the Oyster [31], installed between 10 and 20 meters deep (nearshore). This model is larger than the WAVEROLLER and contains good robustness, with a reduction in maintenance costs. It uses a hollow steel structure that oscillates with the passage of waves, and at its base it has hydraulic cylinders that are responsible for pressurizing a fluid to a central station located on the coast. This fluid feeds a hydraulic actuated generator that is responsible for producing electricity. The fluid is cyclically channeled back through a low-pressure pipe to the offshore system.


*Figure 19 - OYSTER [31]*

### 2.3.3. Terminators – Overtopping Devices

In the class of overtopping devices, it is worth mentioning, the CETO [32] which consists of pumping, through the linear movement of the floating body, a high-pressure fluid to a generator located on the coast that uses the pressure difference as a way to of energy source. This technology is divided into two substations. The CETO I, which is a reverse osmosis or hydroelectric substation, includes a submerged actuator connected to a

pressurized fluid circuit using the swell of the sea wave. This energy is collected from all devices before being fed back to the CETO II substation, which in turn converts energy located on land.

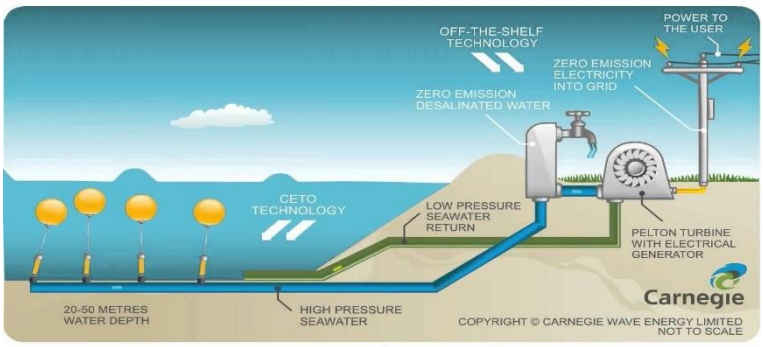


*Figure 20 - CETO [32]*

In the same class, the company Aquaret® developed the Wave Dragon [33] designed to be installed at a depth of more than 20 meters. The mode of operation is identical to the production of water in hydroelectric dams in rivers. The structure of this type of system is floating, where the ramp with double curvature collects and directs seawater into a reservoir located at a higher level, in order to increase the potential energy associated with its mass. Then, the water passes through a turbine connected to a permanent magnet generator in order to minimize losses, to return to the sea.

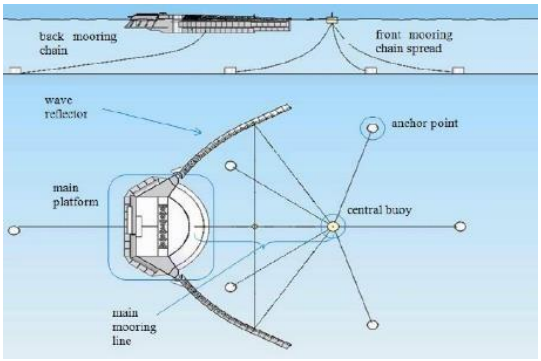


*Figure 21 - Wave Dragon [33]*

The company Weptos [34], uses rotation mechanisms identical to the Salter's Nodding Duck device capable of transmitting the movement through hydraulic cylinders to transform kinetic energy into potential energy.

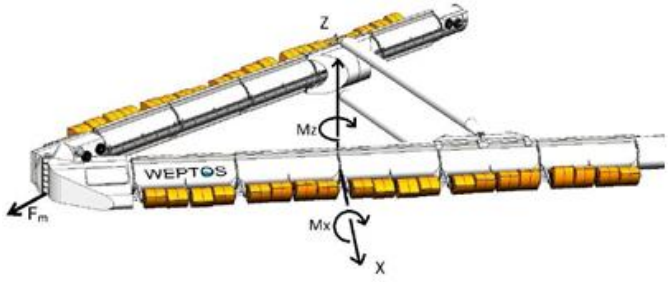


*Figure 22 - Weptos [34]*

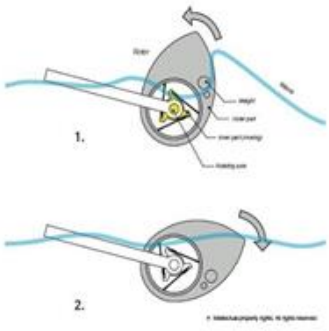


*Figure 23 - Salter's Nodding Duck [34]*

In this case, we can observe the use of pneumatic cylinders used in the rotation mechanisms, identical to the Salter's Nodding Duck device, which provide pressure in a rotating manner in three different phases, exerting continuity in the production of energy in regular waves in favorable situations. In this case, it is necessary the presence of a force in an axis that guides in the direction of the waves, in order to facilitate the regularity of the input of the maritime resource.

The Seawave Slot-Cone Generator (SSG) system [35] is an overtopping system that uses multiple superimposed reservoirs, built in concrete, so that, in this way, the fluid passes from reservoir to reservoir, transferring the potential energy to a multi-stage turbine.

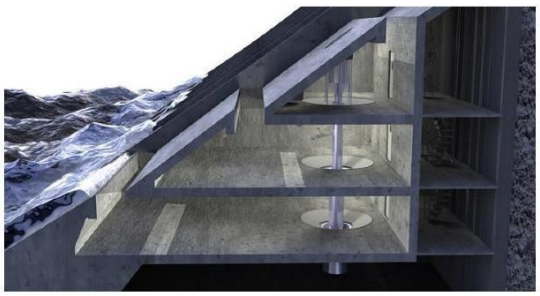

*Figure 24 - Seawave Slot-Cone Generator [35]*

The Tapchan [26] is an old system based on a partially submerged structure. This structure forces the water mass to be overtopped by a ramp to a reservoir that is above the midline of the sea. This mass is returned to the ocean by pipelines. The turbines installed in these pipelines are responsible for energy conversion.

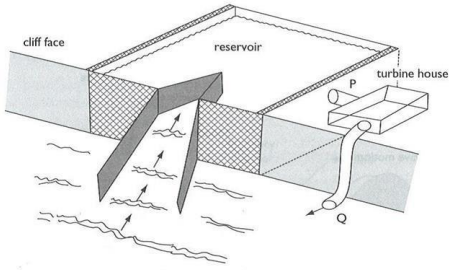


*Figure 25 - Tapchan [26]*

### 2.3.4. Point Absorbers – Heaving Point Absorber (HPA)

In the class of HPA, we can mention the Archimedes Wave Swing [36] developed by Teamwork Technology BV®. This technology removes energy through the pressure differential exerted on the air column, which generates a vertical movement, transforming pressure into electrical energy through hydraulic and electromechanical mechanisms. It rests on a submerged hollow steel structure, which supports two concentric cylinders one inside the other, whose relative motion is created by the incident wave action. The lower cylinder is fixed to the seabed, while the upper one moves vertically, inside, between the two cylinders. This type of hydraulic PTO is associated in parallel with a linear generator to produce electricity.

The Powerbuoy [37] uses a hydroelectric turbine and has no restrictions on mooring, that is, it floats along the coast at depths greater than 55 meters. This technology manipulates the energy of the vertical movement of waves between 1 to 6 meters in height. When the sea movement is no longer normal, the system goes into standby.

Figure 26 - Archimedes Wave Swing [36]


Figure 27 - Powerbuoy [37]

The Aquabuoy [38] has a vertically moving buoy mounted. With this movement, a fluid passes through a device located in a second floating body, which is responsible for generating energy through the relative movement of two components. This device easily adapts to the height of the tide due to the flexibility of the moorings. The Aquabuoy 2.0 consists of a 3 meters diameter buoy, connected to a 70 meters long axle.

The Manchester Bobber technology [39] consists of a set of buoys fixed to a metallic structure. Identical to the previous cases, the mechanical energy is generated by the vertical movement of the buoys associated with the movement of the tides that rotates a drum that feeds the generator. To establish dynamic balance in the structure, it is necessary to have a counterweight in order to keep the cable that connects the cylinders to the drum always tense.

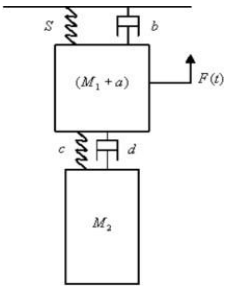


Figure 28 - Aquabuoy schematic [38]

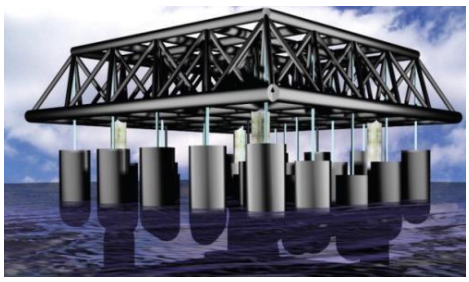

Figure 29 - Manchester Bobber [39]

The Waverider Energy [29] is a WEC that consists of a modular structure in carbon steel, with dimensions of 18 m x 13 m x 4 m. The set of the various modules can reach a maximum dimension of 111 meters and a mass of around 290 tons. This enormous weight results from the density of the metal.

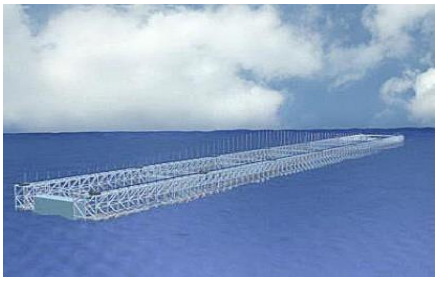

Figure 30 - Waverider [29]

The WEGA [31] (wave energy gravitational absorber) is a technology developed by the Portuguese company Sea for Life®, which consists of a hollow cylinder in fixed steel, through a rotating head with two degrees of freedom of a hydraulic PTO.

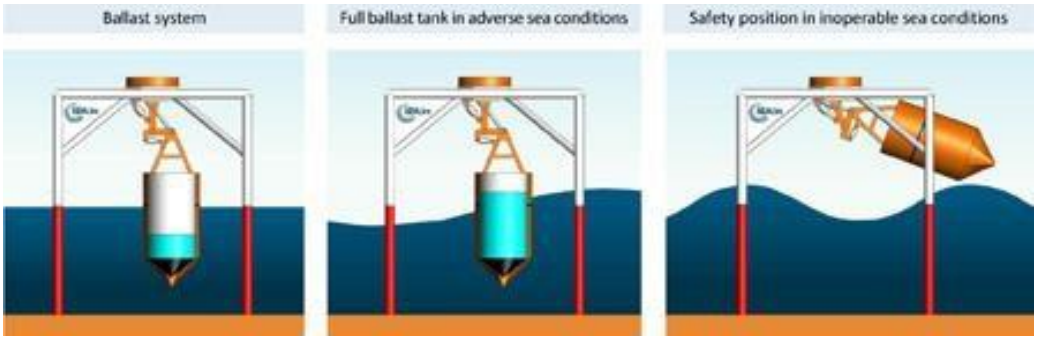


*Figure 31 - WEGA [31]*

The Wavebob [41] uses pistons that pump a pressurized liquid, making it run through a turbine. It is an offshore device that has a damping system for more critical cases of wave movement.

The Wavestar [42], similar to the Waverider, contains twenty hemisphere-shaped buoys, partially submerged, which activate a hydraulic pump. The approaching wave pushes the floats upwards in the order in which they are aligned, which allows the continuity of electrical production. The compressed oil used is collected by pumps associated with each float and fed by a common accumulation system. The disadvantage, compared to floating systems, is the impossibility of moving the structure, which is fixed on two pillars, towards the direction of the wave, resulting in a decrease in its performance. In adverse conditions the floats are raised as a safety mechanism.

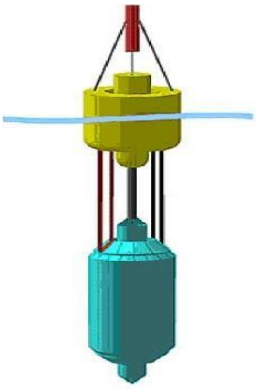

*Figure 32 - Wavebob [41]*

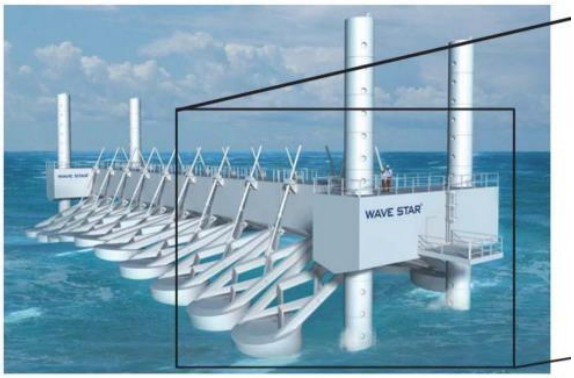


*Figure 33 - Wavestar [42]*

### 2.3.5. Point Absorbers – Oscillating Pitch Absorber (OPA)

In the OPA class, we can mention the SEAREV [43] that is an absorber with a rotation float. It has a pendulum that is inside a hollow body. The wave, when crossing it, causes it to oscillate, and the kinetic energy is absorbed by the pendulum that has coupled some hydraulic systems, which make a fluid circulate through a circuit, that feeds the generator.

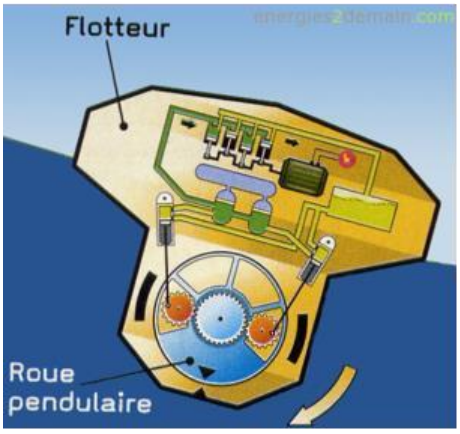


*Figure 34 - SEAREV [43]*

With an asymmetrical design, the Penguin WEC [20] has a total weight of 220 tons and is 30 meters long. It is a semi-submerged ship, with only 2 meters above sea level. Inside there is an eccentric mass, which rotates with the movement of waves. This mass is coupled to a generator, which in turn converts the mechanical (rotational) energy into electrical energy.

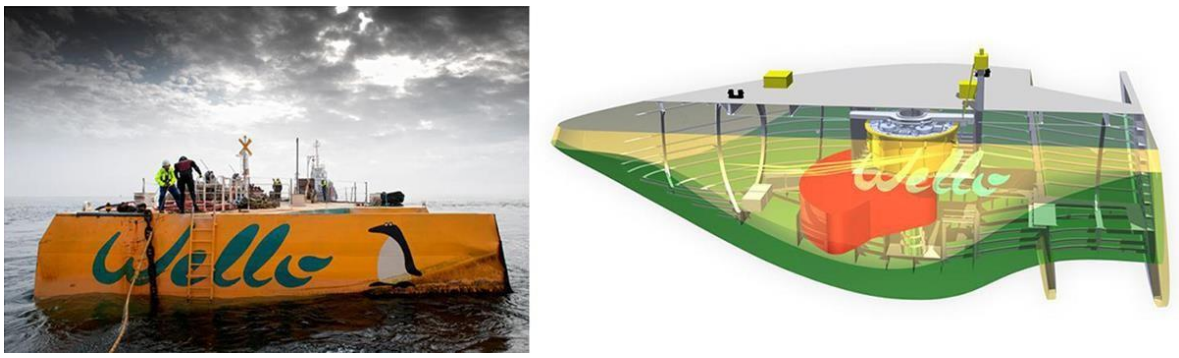

*Figure 35 - Penguin WEC [20]*

### 2.3.6. Attenuators

In the attenuators class, we can mention the Pelamis [20], developed by Aquaret®, in Portugal in Povoa do Varzim/Aguçadoura. It is a semi-submerged steel structure, with 120 meters long and 3.5 meters in diameter. This structure is interconnected by hydraulic joint lines, aligned in the direction of wave propagation.

When the waves hit the structure, each energy conversion module moves on two independent axes that are offset 90° from each other, allowing oscillation to occur in either direction. In the joints, the resistance imposed by the functioning of the cylinders, makes the high-pressure biodegradable oil pump through accumulators for the motors. These hydraulic motors, in turn, drive electric induction generators. The total installed power of the Pelamis P-750 is 250 kW per module. Electricity passes through the modules reaching the bow, where the transformer is installed. The online transformer is responsible for raising the voltage level before connecting to the submarine cable, which is fixed on the seabed.

The McCabe Wave Pump [44] uses the relative movement of the lateral parts that pressurize a fluid. This system was developed by the company Hydam Technology Ltd®, which installed a device in the Shannon Estuary, on the Irish coast.

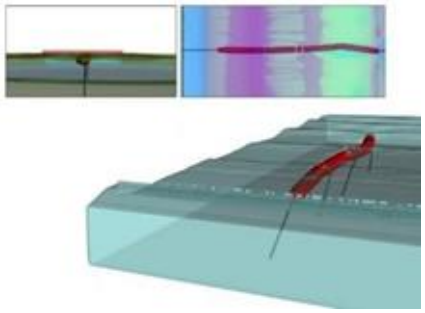

*Figure 36 - Pelamis [20]*

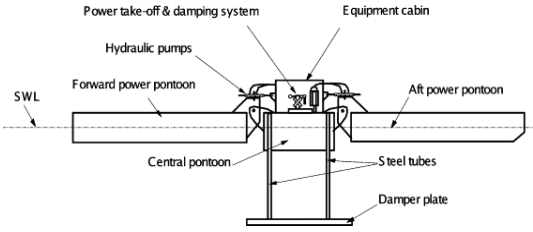


*Figure 37 - McCabe Wave Pump [44]*

The advantage of WEC systems in the attenuators category is the reduction of mechanical damage due to their hydrodynamic design in front of the devices. However, the disadvantage is the need for the permanent existence of wave movement.

### 2.3.7. Modern Prototypes

In the modern prototypes class, we can mention the case of submerged offshore turbines (Figure 38) which takes energy from the sea currents in the high seas.

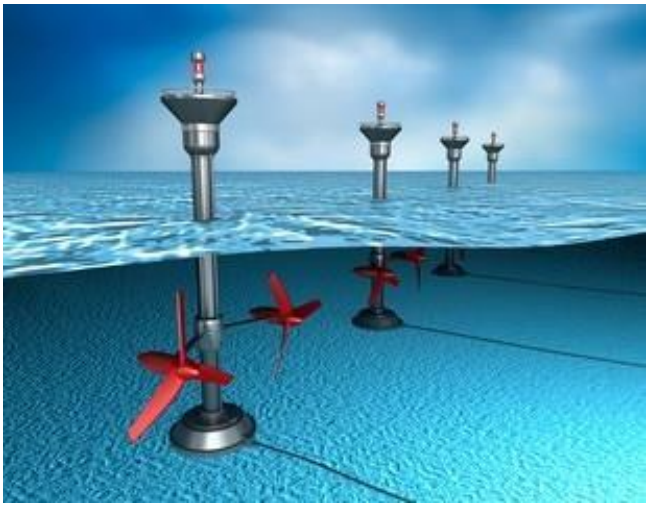

*Figure 38 - Offshore turbines [45]*

The Inertial Sea Wave Energy Converter (ISWEC) [46] consists of a gyroscope, which is inside of a floating capsule, which causes a reaction of the inertia force to the ripple. Inertia forces on the three axes create turbulence in the buoy and the gyroscope tends to counteract the oscillating motion, increasing torque and rotational speed. This mechanism, when found inside a capsule, is protected from seawater corrosion and sediment erosion. As it behaves like a bulky dead body, it resists more easily in adverse situations and presents itself in the category of oscillating step.

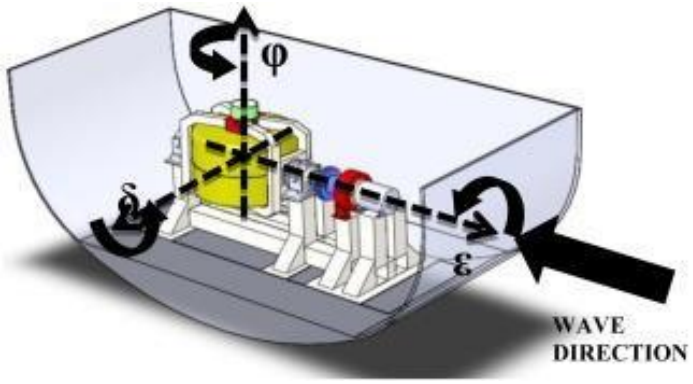


*Figure 39 - ISWEC [46]*

The BLUSphere technology [47] is being developed by the Portuguese company Emove®. It contains a spherical generator inside, capable of capturing the kinetic energy of the wave coming from any direction. Such a system with 3 meters in diameter is capable of producing 500 kW.


*Figure 40 - BLUSphere [47]*

The Waveline Magnet WEC (WM7) [48] uses electromagnetic force to produce high-efficiency electrical energy at low cost. This device is neutral in terms of buoyancy and adheres to the surface of the water, so it precisely follows the contour of the wave as the wave passes through. This buoyancy translates into an impact on the useful life of this technology, being a bonus factor for implementation in the ocean.

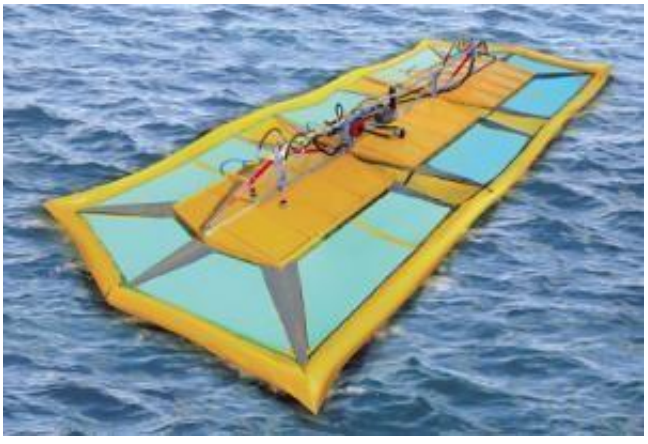

*Figure 41 - Waveline Magnet WEC [48]*

## 2.4. Power Take Off (PTO)

The transformation of kinetic or potential energy from sea waves (mechanical energy) into electrical energy can be done in several ways:

- turbines in which they supply mechanical energy to rotating electrical generators;
- hydraulic systems in which the movement is slow but powerful;
- mechanical systems consisting of a series of mechanical components to convert oscillating motion (which is linear motion) into rotational motion to then power an electrical generator;
- and linear generators.

### 2.4.1. Turbines

This conversion system is used in fixed structures, such as hydro stations or wind farms. The part of the station that is on the ground uses synchronous generators that operate at a constant speed, equaling the frequency of the grid.

In the turbines, there is a non-linearization of the energy input from the sea, but this is solved through the introduction of a gearbox or through electronic converters that convert the current to DC current and back to AC current in order to equalize the voltage and the frequency of the grid. Turbines are expensive and can cause power losses, but they allow the obtainance of large amounts of energy over the time they operate.

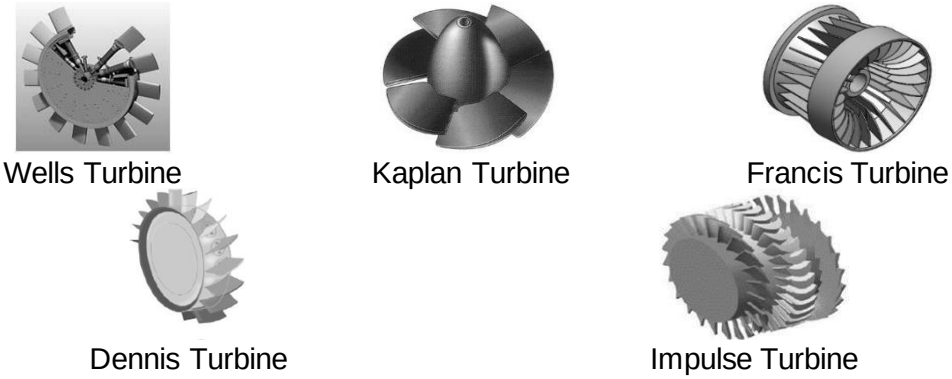


*Figure 42 - Types of turbines [52]*

### 2.4.2. Hydraulic Systems

The slow but powerful movement of waves is ideal for these systems. The movement of the waves pressurizes the oil in a reservoir that then feeds an electrical generator. [49]

This system captures the movement of waves, through the interaction of the actuator and the high-pressure fluid inside double-acting hydraulic cylinders. This movement will trigger the directional valves (to detect the direction of fluid movement at high pressure) reflecting the movement of the hydraulic motor. The advantage of this motor is the ability to provide the generator with a constant speed. However, the use of accumulators in the mechanical system will be to regulate and store the energy derived from the movement of the fluid to the hydraulic motor.

Overall, hydraulic PTO appears to be a good solution on paper, but it is quite limited in the real world due to its complex systems and difficult operating conditions.

### 2.4.3. Direct Mechanical Drive Systems

The direct mechanical drive systems consist of a series of mechanical components (pulleys, gears or screws...) to convert oscillating motion (which is linear motion) into rotational motion to then power an electrical generator. These systems can often be integrated with a flywheel to smooth out erratic wave motion [21].

The requirements for such a device are extremely high and, as a result, its real-world feasibility is still under debate [21]. Although several smaller prototypes were built and tested.

### 2.4.4. Electric Generators (Rotating Electrical Machines)

Rotating electrical machines are made up of two distinct parts: the stator and the rotor.

The stator (fixed part of the machine) consists of a housing that supports a core, generally made of stacked and isolated magnetic plates, provided with holes where a set of three windings is mounted (one for each phase in case of a three-phase system) arranged symmetrically [53].

The rotor (moving part of the machine) is placed inside the stator, having the shape of a cylinder for this purpose. Like the stator, the rotor consists of a magnetic core and three windings offset by 120º (in case of a three-phase system). This magnetic core is supported under the shaft, normally in steel. The rotor windings can have two types of construction: squirrel-cage or wound [53].

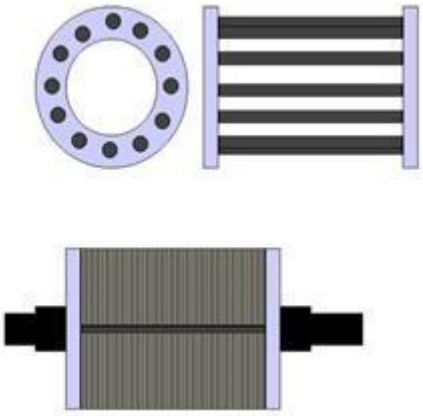

*Figure 43 - Schematic of a simple squirrel cage rotor [54]*

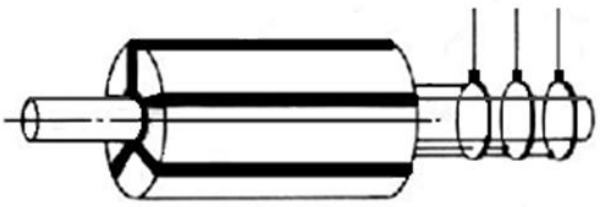

*Figure 44 - Schematic of a wound rotor [54]*

For the production of electrical energy, these rotating electrical machines are used as generators. In this sense, there are three types of synchronous generators used: doubly-fed induction generators, cage induction generator and permanent magnet synchronous generators.

In the case of the Doubly-Fed Induction Generator (DFIG), these can control the current and voltage in the motor keeping the generator running in sync with the grid, because they have a wound rotor whose rotor circuit, which operates at a variable frequency, is connected to the grid (characterized by a fixed frequency) through an AC-DC-AC frequency converter, visible in Figure 45. The generator's electromotive force, generated by the air current, makes it possible to increase and decrease the speed in two directions.

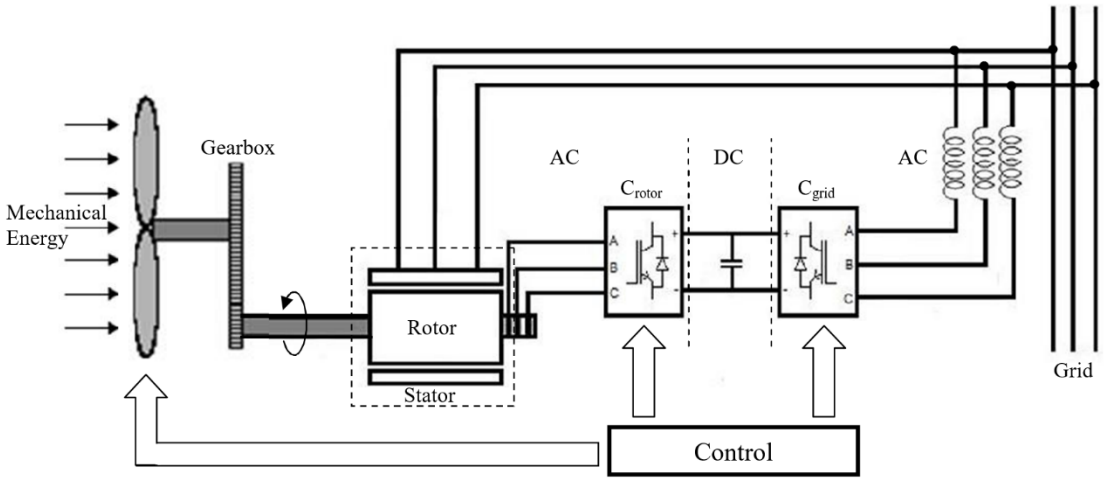


*Figure 45 - Schematic of a DFIG (adapted from [55])*

However, this type of generator has its drawbacks, firstly, it requires an additional starter unit to gradually power the generator at the right speed, protecting it from power surges. In addition to their starting procedure, the fixed speed nature of these systems implies the use of a complex PTO to convert irregular motion into fixed speed. Hence the common presence of these generators in hydraulic systems, which with their displacement manipulation are able to guarantee the required speed [49].

### 2.4.5. Linear Generators

This more modern type of PTO offers a lower need for maintenance, lower costs and possible short-term profitability compared to the two previous types. This conversion method is used in WECs such as Archimedes Wave Swing and Powerbuoy, representing the direct conversion of movement along an axis of action. The generators have the following characteristics: flat geometry, double stator, double translator, ferromagnetic core and longitudinal flux.

The concept of this device is the interaction between the fixed part (stator, composed of coils) and the mobile part (translator, composed of permanent magnets placed alternately). The vertical movement caused by the float induces an electric current in the fixed coils [23].

The determining factor of energy efficiency is due to damping. The higher the damping, the lower the electrical production, and the lower the damping, the greater the existing dissipation. Whether in regular waves or irregular waves, it is important to pay attention to the dynamics of the input, and therefore the greater control and compliance of the equipment, the better. This input must be passively rectified via a diode bridge or actively with an electronic rectifier.

In Figure 46, although we see a direct passage from the mechanical energy input to the electrical energy output, this type of generators has an efficiency of only about 40% [50]. It is for this reason that this type of generator is not commonly used and is still under development.

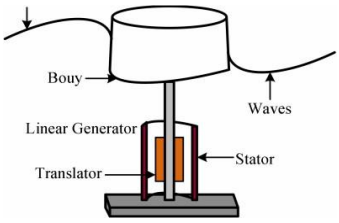


*Figure 46 - Linear generator [23]*

## 2.5. Types of Energy Transport

Electric power can be transported in either AC current or DC current. Depending on the generator in the system, the energy generated from them can be very irregular, both in voltage and current [49].

In fixed speed generators, it is possible to make a direct connection to the grid, thus avoiding expensive converters, requiring only a bank of capacitors, but this can only be done if a careful selection of speed and number of poles is made, so that the generated energy has the same voltage and frequency as the grid [49].

As for variable speed generators, the energy produced is highly irregular and, for this reason, it is necessary to adapt and convert this irregular form of energy into regular grid energy [4] [51]. To perform the conversion, most systems use a combination of AC to DC and then DC to AC converters [49], with the possibility of a battery included in the DC circuit.

With this type of generator, its versatility in a wider operating range of conditions is a notable advantage and together with the DC circuit, there is the possibility of power transmission via High Voltage Direct Current (HVDC).

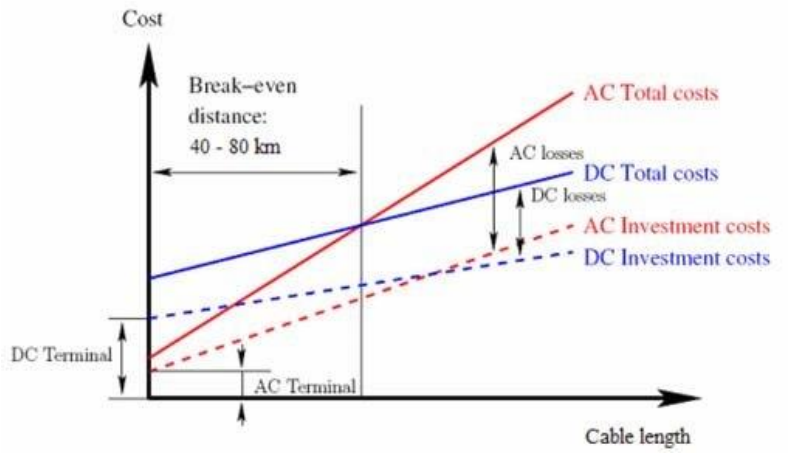


*Figure 47 - Comparison of investment cost for HVAC and HVDC cable transmission [56]*

In Figure 47 we can see that up to a certain distance, it is less expensive to use AC current. From this distance upwards, the use of DC current becomes more profitable.

Intentionally blank page.

# 3. Work Development

The development of this work is related to the development of an AC-DC-AC converter to enable the connection of the generator to the electrical grid, laboratory operation test and evaluation of the behavior and energy characterization of the PTO.

## 3.1. Work Introduction

In order to carry out tests and trials, in this project it was initially necessary to develop a structure (Figure 48 and Figure 49) capable of accommodating the generator and an electric motor, which will be used to simulate the movement of waves on the generator shaft.

*Figure 48 - Rendering of the structure used (including the electric motor and the generator)*

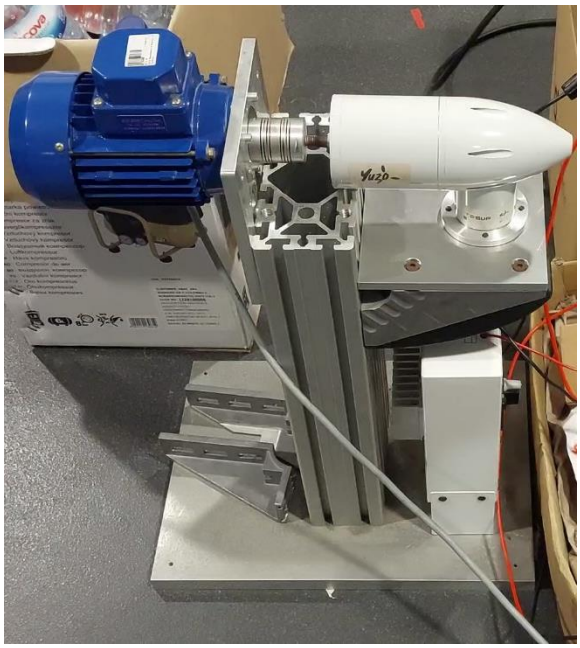

*Figure 49 - Structure used (including the electric motor and the generator)*

This structure is composed of a 90x180 mm aluminum profile attached to an aluminum base, where is attached two 175x175x12 mm aluminum plates that had been machined. The electric motor is attached directly to one aluminum plate and the generator is attached to another aluminum plate using a support piece that also had been machined.

The connection of the electric motor to the generator is made through an elastic mechanical coupler from Norelem. This coupling, after being acquired, had to be machined in order to enlarge the holes to the size of the shafts. On the shaft of the electric motor, due to the existence of a key, a bushing was produced.

The 2D drawings of the structure and the fabricated and machined parts can be found in Appendix A.

## 3.2. Components

In this section, the components used in the development of this work will be explained.

### 3.2.1. Variable-Frequency Drive

The Variable-Frequency Drive (VFD) is an electronic equipment designed to control the speed of alternating current electric motors. The speed variation is obtained by the conjugate variation of voltage and frequency of the current that reaches the electric motor, according to a curve that, in turn, can also be changed by the drive itself.

The VFD used is a Mitsubishi FR-S520S-0.4K-EC. It has a rated input of 200 to 240 V AC single-phase at 50/60 Hz, with an output voltage of 200 to 240 V AC three-phase at 50/60 Hz (variable) and an applicable motor capacity of 0.4 kW.


*Figure 50 - VFD Mitsubishi FR-S520S*

### 3.2.2. Electric Motor

The electric motor used is a M63b4 three-phase asynchronous motor capable of providing a mechanical power of 0.18 kW (0.25 HP). The electric motor nameplate is shown in Figure 52.

*Figure 51 - Representative image of the electric motor*

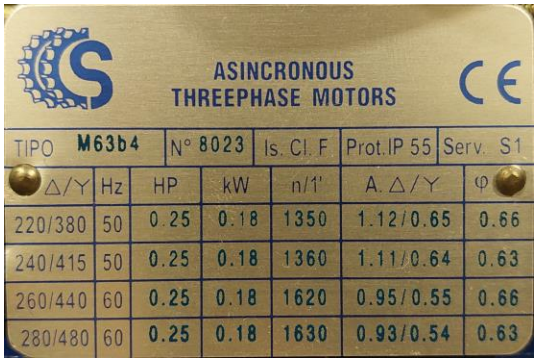


*Figure 52 - Nameplate of the electric motor*

### 3.2.3. Electric Generator

The selection of the generator was made in a previous master's dissertation [8]. The generator is a Tesup Yuzo, a small generator suitable for the production of electrical energy from kinetic energy of wind.

This generator is of the permanent magnet rotor type and, according to the manufacturer, this generator is capable of outputting 300 W at 1000 RPM [57].

To convert the three phase AC current from the generator to DC current, the charge controller of the same manufacturer was previously selected in the same master's dissertation to be used [8].


*Figure 53 - The Yuzo Wind Turbine (on the left) and the Wind Turbine Charge Controller (on the right) [57]*

The controller was used in "inverter" mode, where in that mode the controller only rectifies the three-phase AC current into DC current, similar to Figure 54.

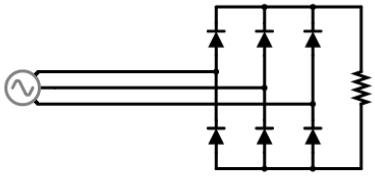

*Figure 54 - Three phase AC to DC rectifier bridge schematic*

### 3.2.4. Boost Converter

The boost converter (step-up converter) is a DC-DC power converter that steps up voltage from its input to its output [59]. It is a switching regulator with a power conversion circuit that works at high frequency [60]. Considering no losses, if the voltage on the output goes up, the current on the output goes down.

The block diagram working principle of this converter is shown in Figure 55.

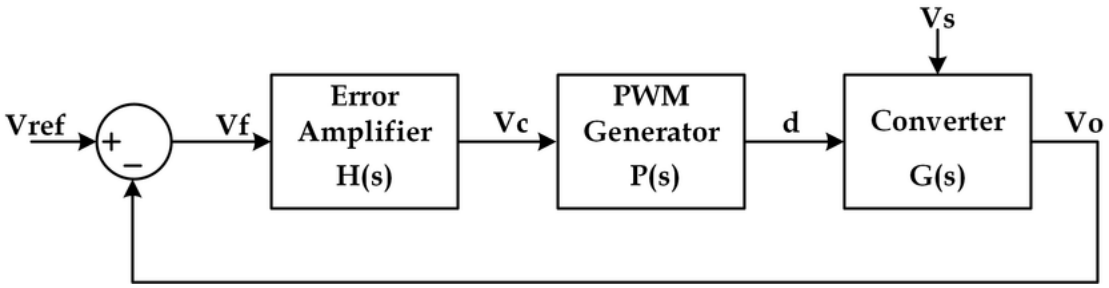


*Figure 55 - Boost converter block diagram [61]*

The converter has a feedback circuit, which, depending on the output voltage read and the intended output voltage, it adjusts the duty-cycle of a PWM signal in order to obtain the desired output voltage.

A boost converter is essentially composed of a coil, a diode, a capacitor and a transistor or a MOSFET. Figure 56 presents the scheme of a boost converter.

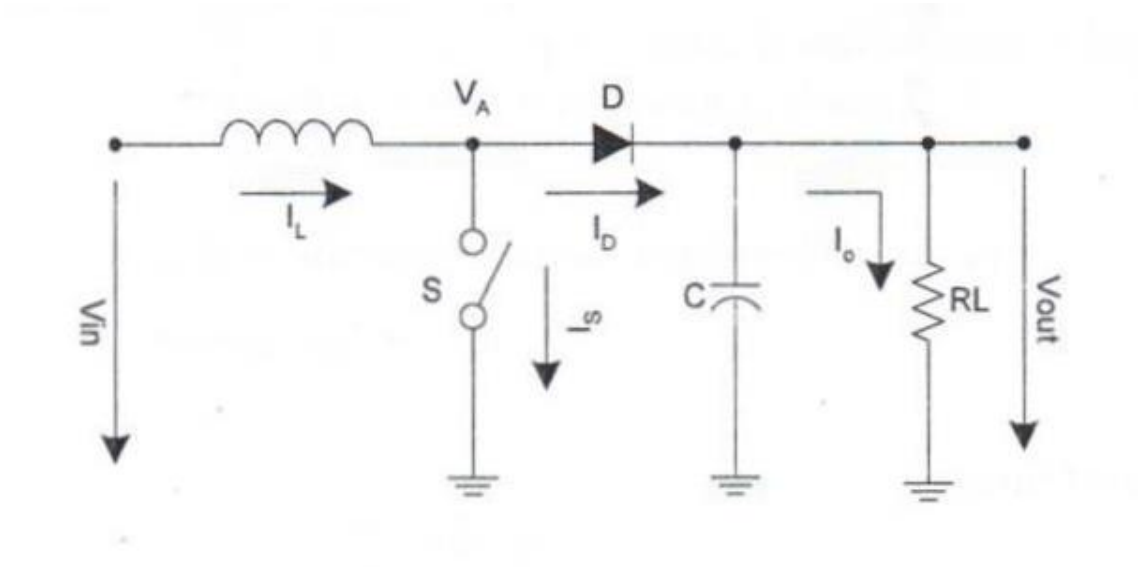


*Figure 56 - Boost converter schematic [60]*

In the previous figure, knowing that the switch $S$ represents a transistor controlled by a PWM signal, it is possible to observe that when the transistor conducts, the voltage applied to the coil terminals is equal to $V_{in}$, so the coil current ($I_L$) increases, accumulating energy, and, in this case, diode $D$ is in reverse bias (because $V_{out}$ is greater than $V_{in}$), so it does not conduct, and therefore the current in the load ($R_L$) is supplied by capacitor $C$ (assuming the circuit has been on for some time). When the transistor does not conduct, the coil current decreases, releasing energy, and therefore, in this case, the diode $D$ goes into conduction (forward bias), making the voltage $V_{out}$ equal to the sum of the voltage $V_{in}$ and the voltage of the coil ($V_L$).

The converter selected and used during the development of the work was a 1500 W boost converter. This selection is due to the operating voltages, in which case, the selected converter can operate with an input voltage between 10 to 60 V DC (from the generator controller), being able to be regulated to an output voltage between 12 to 90 V DC (to the grid-tie inverter).

### 3.2.5. Grid-Tie Inverter

For the development of this work, a grid-tie inverter was chosen instead of an off-grid inverter.

An off-grid inverter is a device that converts DC current into AC current, which can produce a square wave or a sine wave nearly pure, modified or pulsed (Figure 58), depending on the circuit design [62]. This type of inverter cannot be connected to the mains due to the signals not being exactly the same and due to the lack of synchronism of the signals.

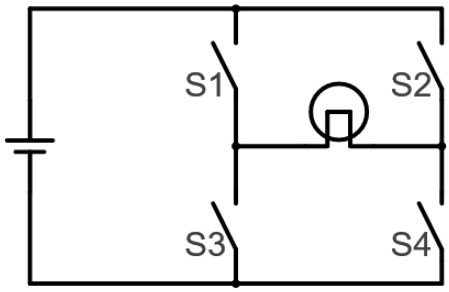


*Figure 57 - Off-grid inverter schematic*

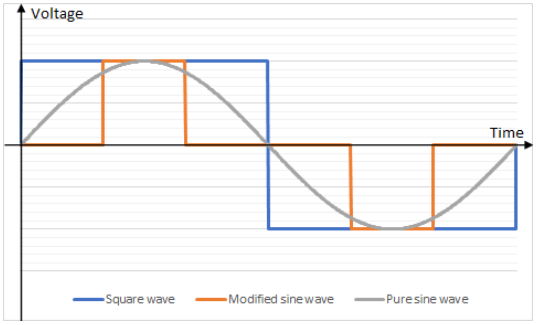


*Figure 58 - Types of the generated inverter waveforms*

The basic operation of an off-grid inverter can be seen in Figure 57. In order for the current to be converted from DC to AC, and using the conventional direction of electric current from positive to negative, if in a first phase the switches $S1$ and $S4$ are closed and if the switches $S2$ and $S3$ are open, the current in the lamp will flow from left to right. If in a second phase the switches $S1$ and $S4$ are opened and the switches $S2$ and $S3$ are closed, the current in the lamp will flow from right to left. If this procedure is repeated fifty times per second, a square wave alternating current of 50 Hz will be obtained in the lamp. The high voltage at the inverter output can be obtained at the DC level with a boost converter, or at the AC level with a transformer [63].

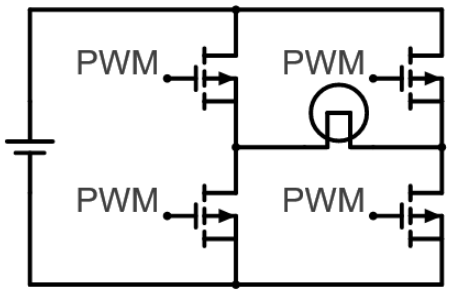


*Figure 59 - Off-grid inverter schematic with transistors*

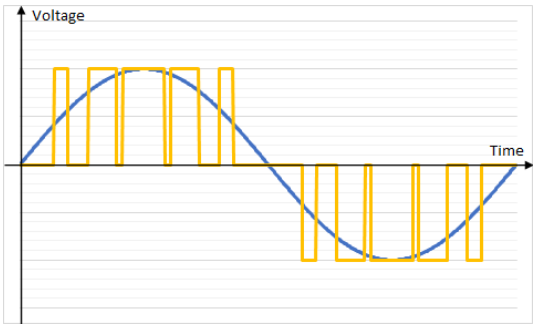


*Figure 60 - Modified sine wave with PWM*

If the switches are replaced by transistors (Figure 59) and if they are controlled with PWM signals, the output current will be a nearly pure sine wave (Figure 60).

A grid-tie inverter is also a device that converts DC current into AC current, but it does not produce any signal at the output, being necessary to be connected to the electrical grid so that the inverter is synchronized with the electrical grid.

For the prototype of this work, the 4SUN 250W/20-50 microinverter was selected, because the maximum power of the chosen generator is 200 W according to the manufacturer. The selected inverter has an input voltage range between 20 and 50 V [65].


*Figure 61 - Microinverter 4SUN 250W/20-50 [64]*

### 3.2.6. Arduino Sensors

For data acquisition, an Arduino microcontroller with several voltage and current sensors was used to obtain the value of the instantaneous electrical power to later calculate the efficiency of the system. The Arduino was chosen because it satisfies the needs of the project.

To obtain the current, both in AC and DC, the ACS712 current sensors [66] were used. For the maximum power value of 200 W, as in the AC part we have voltages around 230 V of effective value, using equation 1 we will have currents in the order of 0.87 A, so for this case we used the 5 A version of the sensor which is currently the lowest version of this sensor, in order to achieve greater sensitivity. As in the DC part we have voltages from 12 V, for the same power value, using equation 1 we will have currents in the order of 16.67 A, so in this case the 30 A version of the sensor was used.

$$P = V \cdot I \tag{1}$$

These current sensors read through a Hall effect sensor, then give an output value between 0 and 5 V, which will be read by the Arduino through an ADC input. As the sensor reads currents in both directions, when the measured current is 0 A, the output value is 2.5 V (half the value between 0 and 5 V).

To obtain the AC voltage, the ZMPT101B voltage module [67] was used, which is composed of a high-precision voltage transformer and an opamp circuit to process the signal to be later read by the Arduino.

To obtain the DC voltage, a simple voltage divider with two resistors was used, as in Figure 64. Knowing that in a voltage divider, the current flowing in the two resistors is equal, based on Ohm's law (equation 2), we can deduce equation 3. Because in the DC part we have voltages up to 50 V, a resistor of 100k Ohms and another resistor of 10k Ohms were used, giving a value of 4.5 V, a value that can be safely read by the Arduino ADC.

$$V = R \cdot I \tag{2}$$

$$V_2 = V_S \cdot \frac{R_2}{R_1 + R_2} \tag{3}$$

*Figure 62 - ACS712 current sensor*

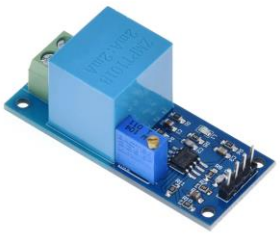

*Figure 63 - ZMPT101B voltage module*

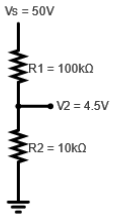


*Figure 64 - Voltage divider*

## 3.3. Tests and Trials

The tests and trials of this work were performed according to the block diagram shown in Figure 65. The electrical diagram can be found in Appendix B.

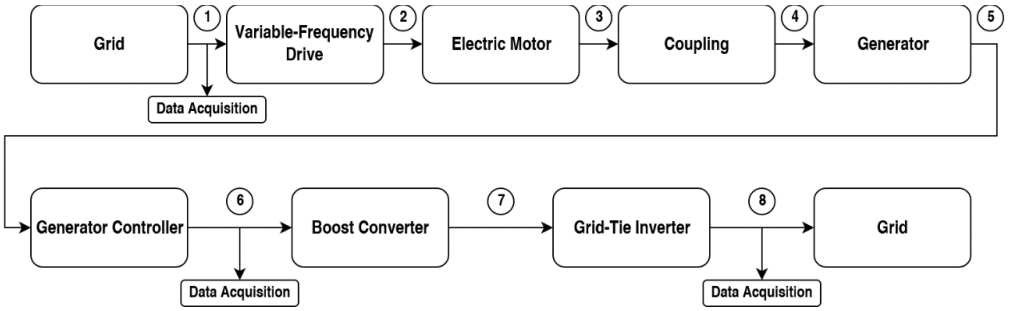


*Figure 65 - Block diagram*

As stated in section 3.1, the electric motor is used to simulate the movement of waves. For the simulation of waves, it was used the same Arduino used in the data acquisition.

In the data acquisition, point 1 was used instead of point 2, because at point 1 we have a single-phase AC current while at point 2 we have a three-phase AC current.

The VFD of the electric motor has a DC voltage analog input to control the electric motor speed and the Arduino has a PWM digital output. Because of that, it was necessary to develop a low-pass filter (Figure 66) in order to convert the digital signal into an analog signal (which works like a DAC).

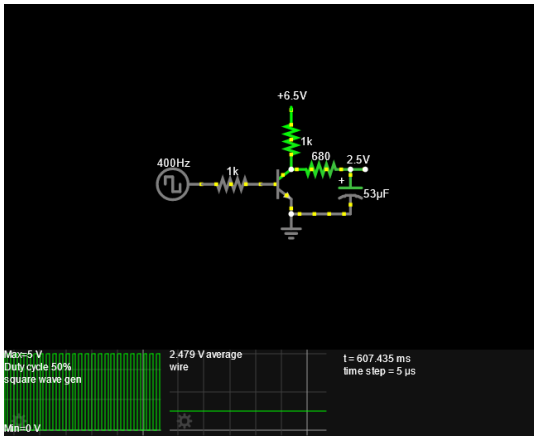


*Figure 66 - Simulation of a low-pass filter using the Circuit Simulator Applet by Falstad*

In the low pass filter circuit, the voltage that is above the resistor that is in the transistor's collector had to be supplied with an external power supply regulated to about 6.5 V (slightly above 5 V) so that when the transistor is at cut off, with the voltage drop of the resistors, the output of the circuit is about 5 V, as intended.

After that, the VFD was programmed so that the speed control of the electric motor is done through an external signal, in this case, the signal from the low-pass filter.

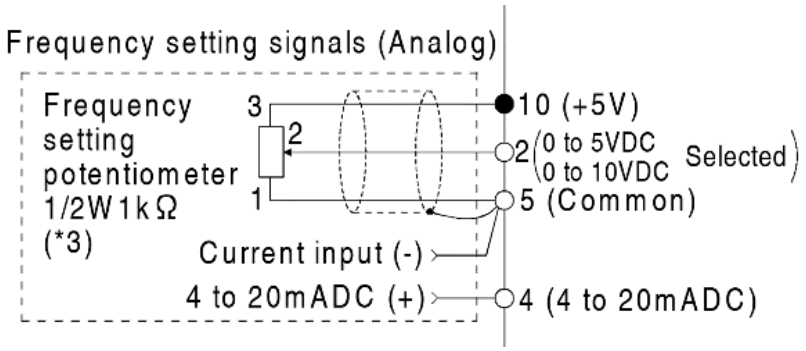


*Figure 67 - Frequency setting signals of Mitsubishi FR-S520S VFD [68]*

Taking into account the VFD's instruction manual, the output of the low-pass filter was connected to pin 2 of the VFD and the ground of the low-pass filter was connected to pin 5 of the VFD, not being necessary to connect the pin 10 because, as explained above, the low-pass filter circuit is powered by an external power supply.

In Arduino program, to control the VFD of the electric motor, a function was used that generates a PWM signal with a certain duty-cycle (adjusted by a program variable), giving the signal seen in Figure 68, captured by an oscilloscope. In the program, another variable was also created in order to change the frequency of the simulated sea wave.

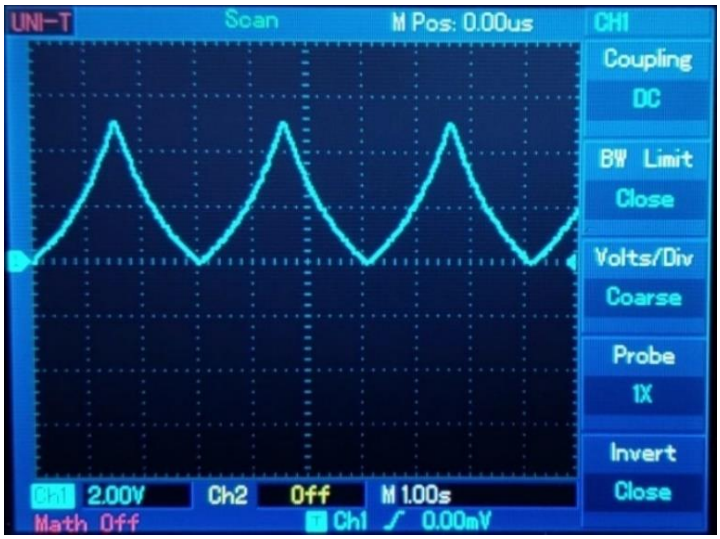


*Figure 68 - Simulated sea wave*

For data acquisition, as current sensors make an instantaneous reading of the current, if this current is AC, according to the Nyquist Theorem, it is necessary that the sampling rate is at least twice the value of the maximum frequency reached by the analog signal to enable digital recording of all analyzed frequencies [69]. Therefore, the data acquisition in Arduino was done with a period of 1 ms. Then it was necessary to calculate the RMS value in order to obtain the effective value of the current.

The code used in Arduino can be found in Appendix C.

The boost converter is used because during the tests of the generator without the boost converter, it was noticed that the grid-tie inverter would shut down when the generator speed reached low RPM. Then it was verified with a magnetic contact to measure the RPM that the generator at about 450 RPM generates a voltage of 20 V DC in open circuit, which is the minimum operating voltage of the grid-tie inverter.

Using an external power supply, the boost converter has been adjusted so that with an input voltage of 12 V (which is within the ranges of the generator controller), its output voltage is approximately 24 V, so that in this way it is possible to keep the grid-tie inverter online with lower RPM. An evaluation of the behavior of the output voltage of the boost converter (adjusted to 24 V) was also carried out as a function of its input voltage, resulting in Graph 1.

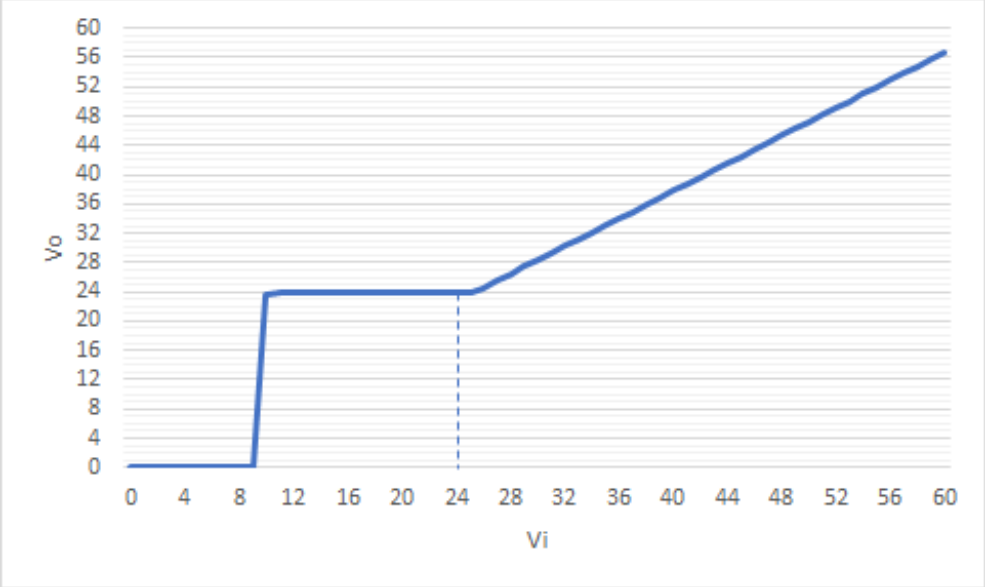


*Graph 1 - Output voltage in function of input voltage of boost converter*

With the use of the boost converter (powered by the system), it was verified that the gridtie inverter did not turn off at low RPM, and could remain online even if the generator was stopped for about five seconds, due to the energy stored in the boost converter capacitors.

## 3.4. Results

For the tests and trials, as sensors were not used to measure the mechanical power supplied to the system, the electrical power entering the system was then measured (point 1 of the block diagram in Figure 65) and it was taken into account that the efficiency of the VFD is around 90% average and the efficiency of the electric motor is around 80% average [70] [71], giving:

$$P_3 = P_1 \cdot 90\% \cdot 80\% = P_1 \cdot 72\% \quad (4)$$

Knowing that the controller is just doing the rectification of the signal coming from the generator to DC current, knowing that in the rectification there are two diodes in conduction simultaneously (for each phase), there will be a voltage drop in the diodes.

As diodes normally have a voltage drop of 0.7 V, in the full-wave rectifier bridge there will be a voltage drop of 1.5 V. As in the DC circuit at the controller output we have voltages around 30 V, this voltage drop corresponds to a loss of about 5%.

In AC, as we have an alternating current (Figure 69), the measurement of voltage and current was made with the Arduino and its sensors, as mentioned in section 3.3.

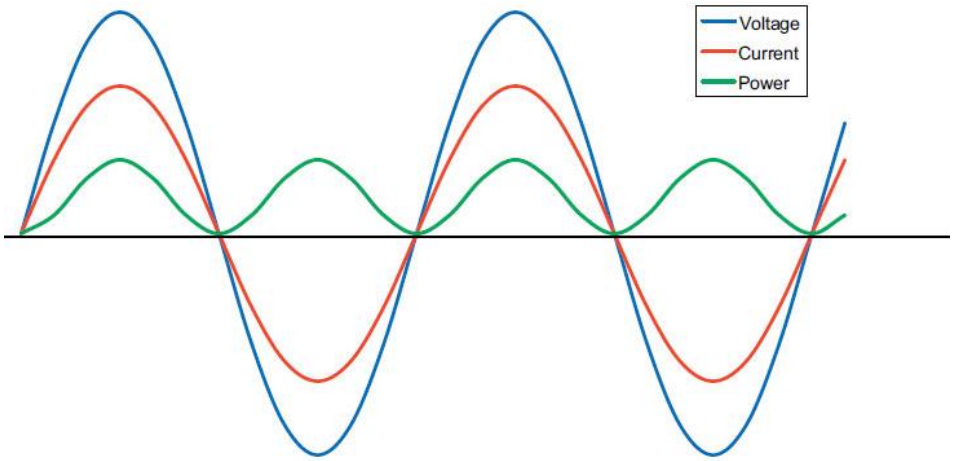


*Figure 69 - Voltage and current in AC [72]*

With this data acquisition, the active power value is calculated by multiplying the instantaneous voltage value with the instantaneous current value with a period of 1 ms:

$$P_i = V_i \cdot I_i \quad (5)$$

Then the average of active power values is calculated with a period of 20 ms:

$$P = AVERAGE\,(P_i) \quad (6)$$

In the first two tests, data were obtained for two situations with a constant VFD frequency value for the electric motor, in Graph 2 for 30 Hz and in Graph 3 for 60 Hz, with a duration of 10 seconds.

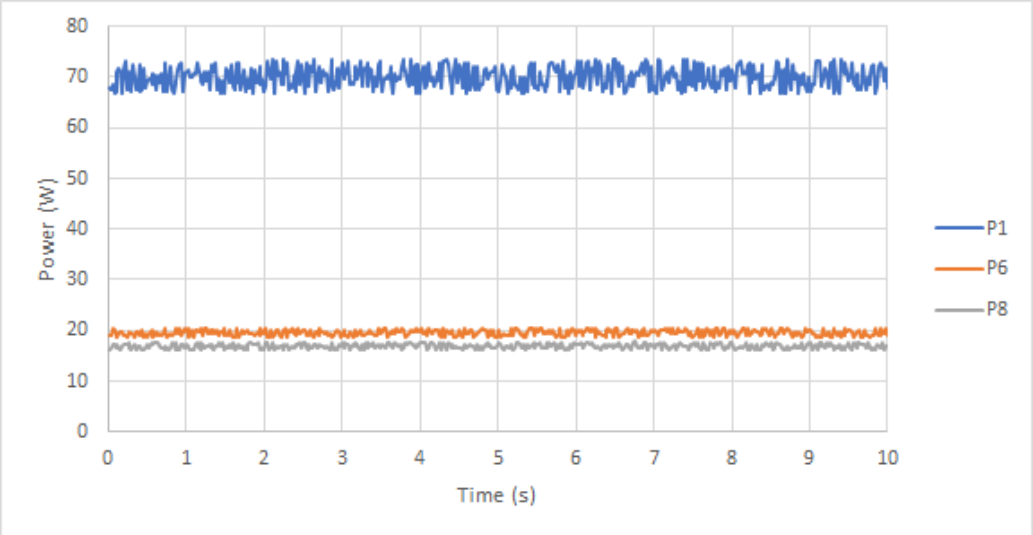


*Graph 2 - Test with constant VFD frequency value at 30 Hz*

Calculating the electrical powers using equations 5 and 6, we have:

$$P_1 = 70.1\,W;\ P_6 = 19.6\,W;\ P_8 = 17.0\,W$$

Knowing that the efficiency from point 1 to point 8 is calculated according to equation 7,

$$\frac{P_8}{P_1} = \eta_{VFD} \cdot \eta_{Electric\_Motor} \cdot \eta_{Coupling} \cdot \eta_{Generator} \cdot \eta_{Generator\_Controller} \cdot \eta_{Boost\_Converter} \cdot \eta_{GTI} \quad (7)$$

we can then deduce the efficiency of the generator (and the coupler), which in this case is about $\frac{P_5}{P_3} = 40.9\%$.

From the values obtained, it is possible to calculate the efficiency of the boost converter and the grid-tie inverter, which in this case is $\frac{P_8}{P_6} = 86.7\%$.

Knowing the efficiency of the VFD and the electric motor, we can estimate the mechanical power supplied to the system, which is $P_3 = 70.1 \cdot 72\% = 50.5\ W$.

In this way, it is possible to determine the efficiency of the system from the input of mechanical energy to the production of electrical energy in the grid, which is $\frac{P_8}{P_3} = 33.7\%$.

In the case of the test with constant VFD frequency value at 60 Hz, we have the following results:

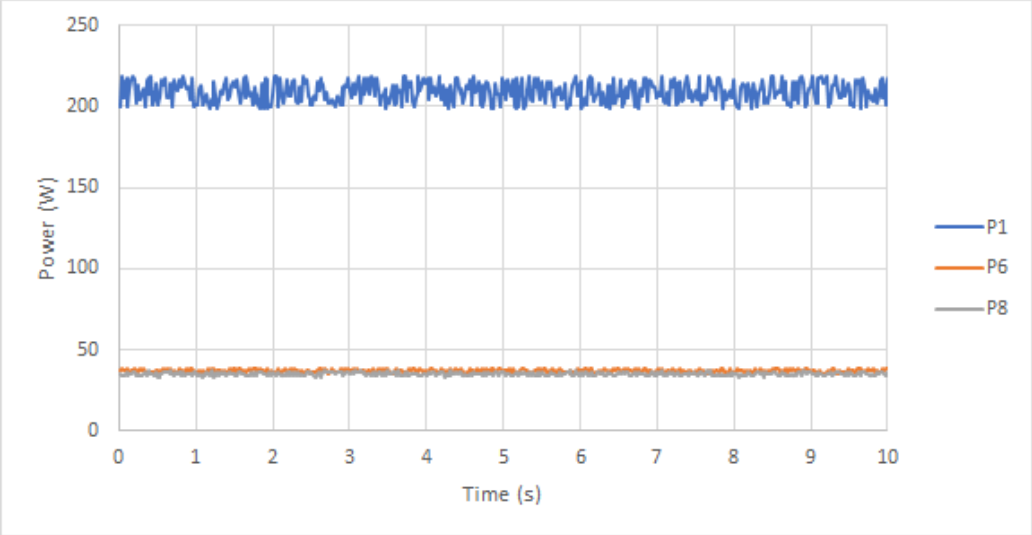


*Graph 3 - Test with constant VFD frequency value at 60 Hz*

Calculating the electrical powers using equations 5 and 6, we have:

$$P_1 = 208.8\ W;\ P_6 = 37.1\ W;\ P_8 = 35.2\ W$$

From equation 7, we can then deduce that the efficiency of the generator (and the coupler) is about $\frac{P_5}{P_3} = 26.0\%$.

From the values obtained, it is possible to calculate the efficiency of the boost converter and the grid-tie inverter, which in this case is $\frac{P_8}{P_6} = 94.9\%$.

Knowing the efficiency of the VFD and the electric motor, we can estimate the mechanical power supplied to the system, which is $P_3 = 208.8 \cdot 72\% = 150.3\ W$.

In this way, it is possible to determine the efficiency of the system from the input of mechanical energy to the production of electrical energy in the grid, which is $\frac{P_8}{P_3} = 23.4\%$.

For the simulation of waves, periods of 0.5 to 5 seconds were used, having as reference previous works.

For the first test with a simulated wave, a period of 0.5 seconds was used with a duration of 10 seconds, where the results of graph below were obtained:

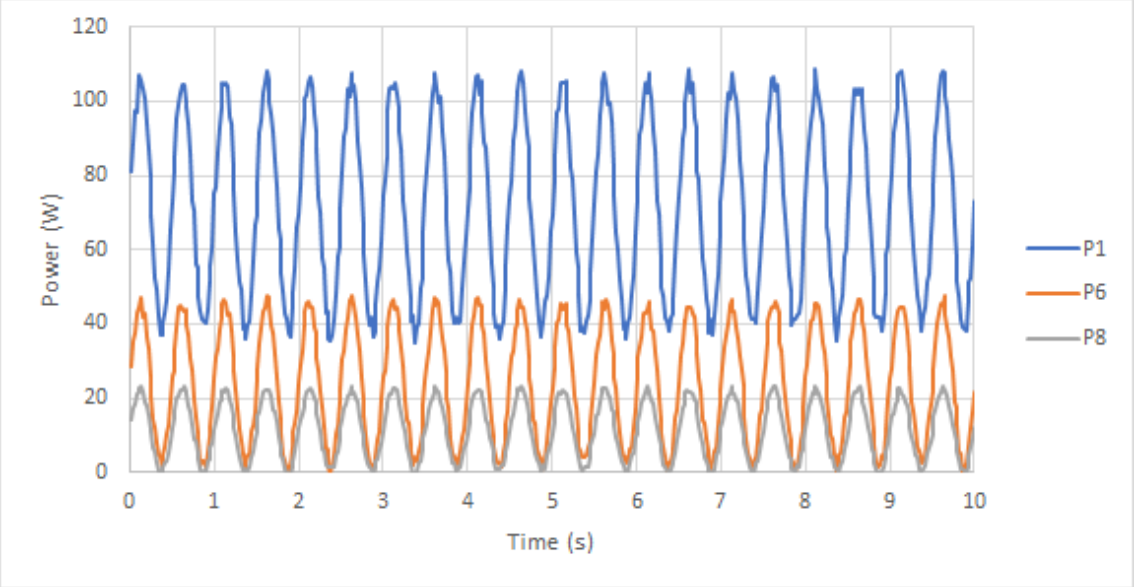


*Graph 4 - Test with a simulated wave with a period of 0.5s*

Calculating the electrical powers using equations 5 and 6, we have:

$$P_1 = 72.0\,W;\ P_6 = 23.8\,W;\ P_8 = 11.5\,W$$

From equation 7, we can then deduce that the efficiency of the generator (and the coupler) is about $\frac{P_5}{P_3} = 48.4\%$.

From the values obtained, it is possible to calculate the efficiency of the boost converter and the grid-tie inverter, which in this case is $\frac{P_8}{P_6} = 48.1\%$.

Knowing the efficiency of the VFD and the electric motor, we can estimate the average mechanical power supplied to the system, which is $P_3 = 72.0 \cdot 72\% = 51.8\,W$.

In this way, it is possible to determine the efficiency of the system from the input of mechanical energy to the production of electrical energy in the grid, which is $\frac{P_8}{P_3} = 22.1\%$.

For the second test with a simulated wave, a period of 1 second was used with a duration of 10 seconds, where the results of graph below were obtained:

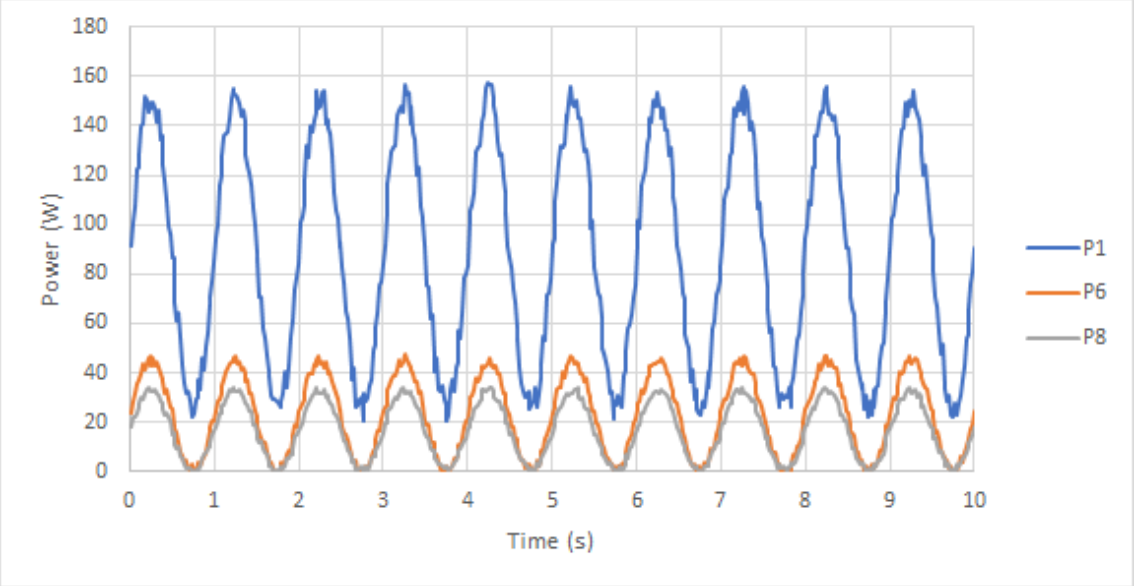


*Graph 5 - Test with a simulated wave with a period of 1s*

Calculating the electrical powers using equations 5 and 6, we have:

$$P_1 = 88.7\,W;\ P_6 = 22.9\,W;\ P_8 = 16.8\,W$$

From equation 7, we can then deduce that the efficiency of the generator (and the coupler) is about $\frac{P_5}{P_3} = 37.7\%$.

From the values obtained, it is possible to calculate the efficiency of the boost converter and the grid-tie inverter, which in this case is $\frac{P_8}{P_6} = 73.2\%$.

Knowing the efficiency of the VFD and the electric motor, we can estimate the average mechanical power supplied to the system, which is $P_3 = 88.7 \cdot 72\% = 63.8\,W$.

In this way, it is possible to determine the efficiency of the system from the input of mechanical energy to the production of electrical energy in the grid, which is $\frac{P_8}{P_3} = 26.2\%$.

For the third test with a simulated wave, a period of 2 seconds was used with a duration of 10 seconds, where the results of graph below were obtained:

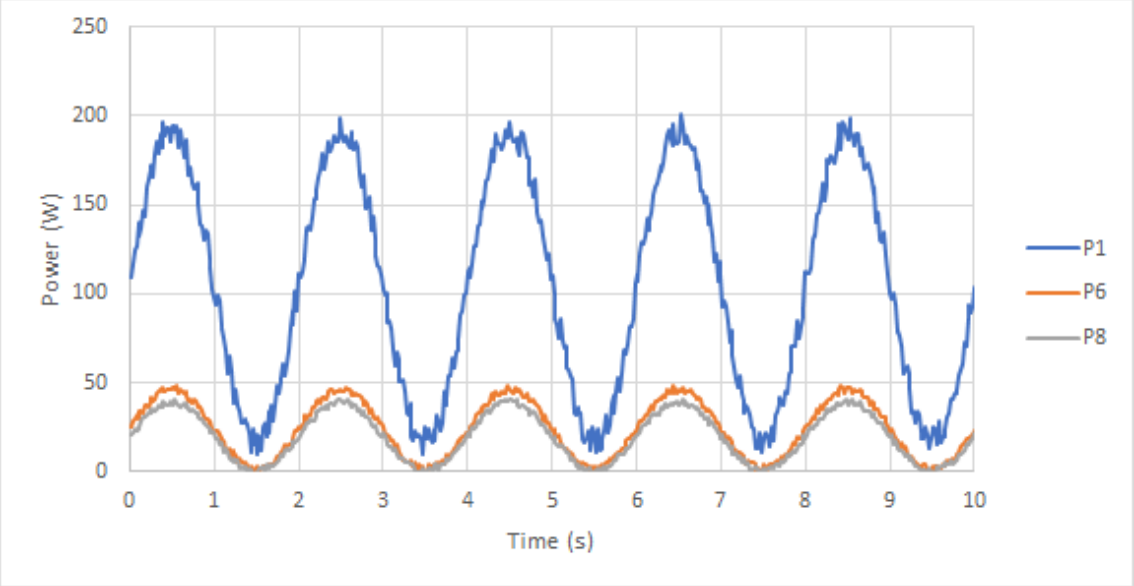


*Graph 6 - Test with a simulated wave with a period of 2s*

Calculating the electrical powers using equations 5 and 6, we have:

$$P_1 = 104.6\,W;\ P_6 = 24.0\,W;\ P_8 = 20.0\,W$$

From equation 7, we can then deduce that the efficiency of the generator (and the coupler) is about $\frac{P_5}{P_3} = 33.6\%$.

From the values obtained, it is possible to calculate the efficiency of the boost converter and the grid-tie inverter, which in this case is $\frac{P_8}{P_6} = 83.0\%$.

Knowing the efficiency of the VFD and the electric motor, we can estimate the average mechanical power supplied to the system, which is $P_3 = 104.6 \cdot 72\% = 75.3\,W$.

In this way, it is possible to determine the efficiency of the system from the input of mechanical energy to the production of electrical energy in the grid, which is $\frac{P_8}{P_3} = 26.5\%$.

For the fourth test with a simulated wave, a period of 3 seconds was used with a duration of 10 seconds, where the results of graph below were obtained:

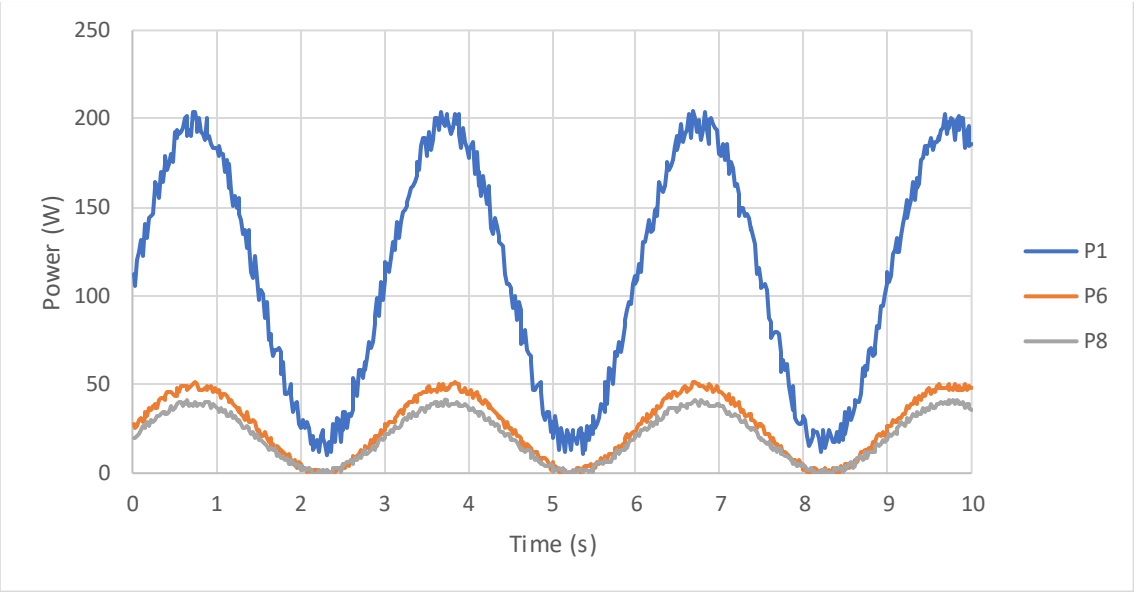


*Graph 7 - Test with a simulated wave with a period of 3s*

Calculating the electrical powers using equations 5 and 6, we have:

$$P_1 = 106.6\,W;\ P_6 = 24.9\,W;\ P_8 = 20.1\,W$$

From equation 7, we can then deduce that the efficiency of the generator (and the coupler) is about $\frac{P_5}{P_3} = 34.1\%$.

From the values obtained, it is possible to calculate the efficiency of the boost converter and the grid-tie inverter, which in this case is $\frac{P_8}{P_6} = 80.8\%$.

Knowing the efficiency of the VFD and the electric motor, we can estimate the average mechanical power supplied to the system, which is $P_3 = 106.6 \cdot 72\% = 76.8\,W$.

In this way, it is possible to determine the efficiency of the system from the input of mechanical energy to the production of electrical energy in the grid, which is $\frac{P_8}{P_3} = 26.2\%$.

For the fifth test with a simulated wave, a period of 4 seconds was used with a duration of 10 seconds, where the results of graph below were obtained:

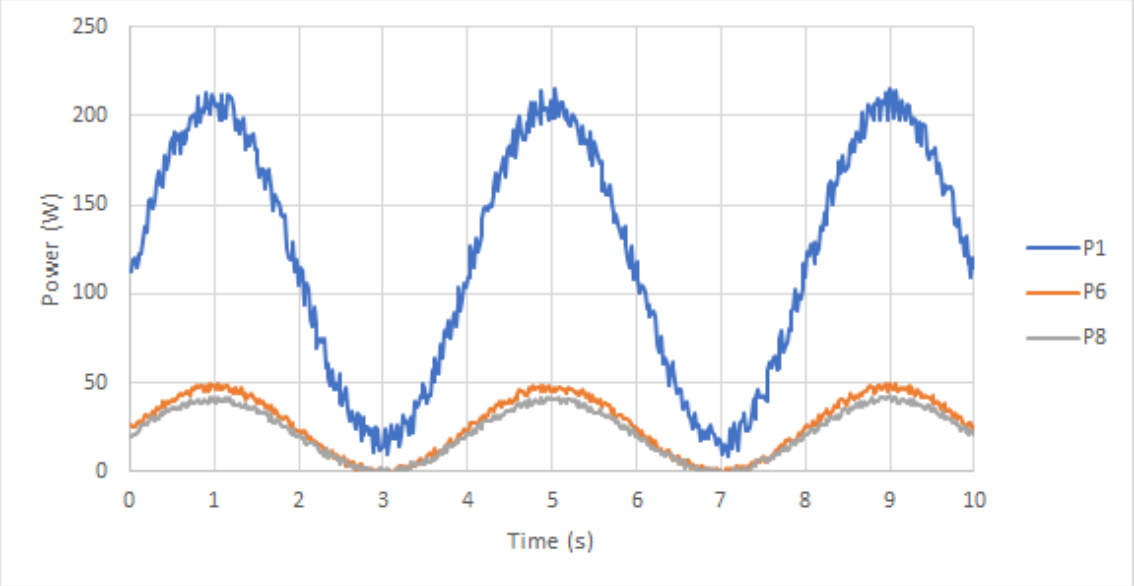


*Graph 8 - Test with a simulated wave with a period of 4s*

Calculating the electrical powers using equations 5 and 6, we have:

$$P_1 = 111.2\,W;\ P_6 = 23.7\,W;\ P_8 = 20.4\,W$$

From equation 7, we can then deduce that the efficiency of the generator (and the coupler) is about $\frac{P_5}{P_3} = 31.2\%$.

From the values obtained, it is possible to calculate the efficiency of the boost converter and the grid-tie inverter, which in this case is $\frac{P_8}{P_6} = 85.8\%$.

Knowing the efficiency of the VFD and the electric motor, we can estimate the average mechanical power supplied to the system, which is $P_3 = 111.2 \cdot 72\% = 80.0\,W$.

In this way, it is possible to determine the efficiency of the system from the input of mechanical energy to the production of electrical energy in the grid, which is $\frac{P_8}{P_3} = 25.4\%$.

For the sixth test with a simulated wave, a period of 5 seconds was used with a duration of 10 seconds, where the results of graph below were obtained:

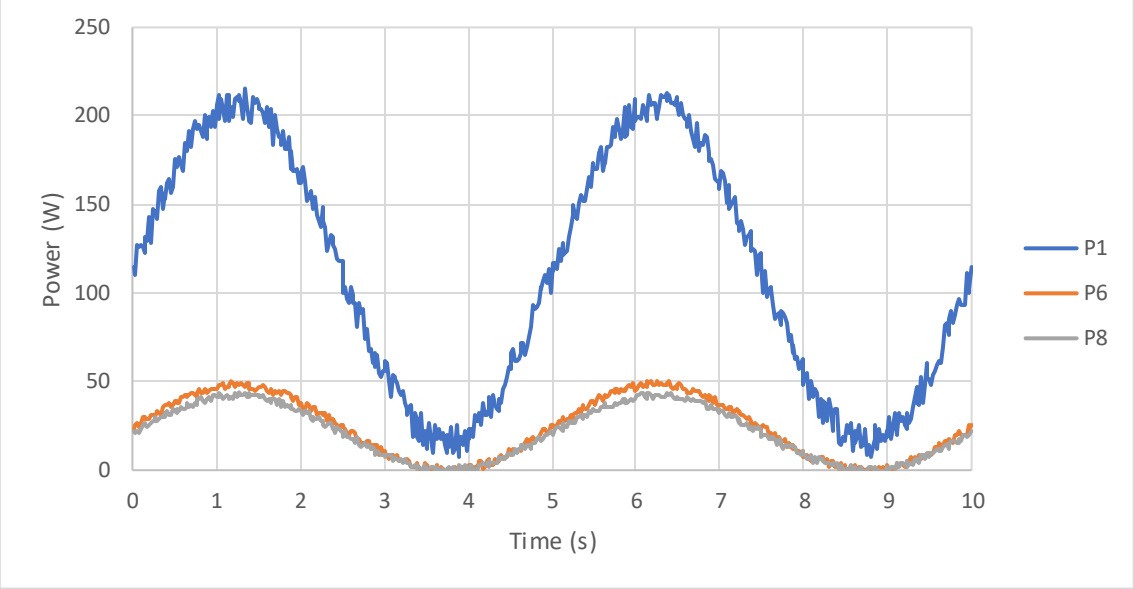


*Graph 9 - Test with a simulated wave with a period of 5s*

Calculating the electrical powers using equations 5 and 6, we have:

$$P_1 = 111.3\,W;\ P_6 = 24.0\,W;\ P_8 = 21.1\,W$$

From equation 7, we can then deduce that the efficiency of the generator (and the coupler) is about $\frac{P_5}{P_3} = 31.6\%$.

From the values obtained, it is possible to calculate the efficiency of the boost converter and the grid-tie inverter, which in this case is $\frac{P_8}{P_6} = 87.5\%$.

Knowing the efficiency of the VFD and the electric motor, we can estimate the average mechanical power supplied to the system, which is $P_3 = 111.3 \cdot 72\% = 80.1\,W$.

In this way, it is possible to determine the efficiency of the system from the input of mechanical energy to the production of electrical energy in the grid, which is $\frac{P_8}{P_3} = 26.3\%$.

From the tests carried out, we can build Table 1 where it is only presented the results of efficiencies of the tests with the simulated wave.

*Table 1 - Efficiencies values of the system from tests and trials*

| Period | Efficiency of the generator and the coupler ($\frac{P_5}{P_3}$) | Efficiency of the boost converter and the grid-tie inverter ($\frac{P_8}{P_6}$) | Efficiency from the input of mechanical energy to electrical grid ($\frac{P_8}{P_3}$) |
|---|---|---|---|
| 0.5 s | 48.4% | 48.1% | 22.1% |
| 1 s | 37.7% | 73.2% | 26.2% |
| 2 s | 33.6% | 83.0% | 26.5% |
| 3 s | 34.1% | 80.8% | 26.2% |
| 4 s | 31.2% | 85.8% | 25.4% |
| 5 s | 31.6% | 87.5% | 26.3% |

From the table above, it is possible to see that the efficiency of the generator (and the coupler) decreases with the increase of the period of the simulated wave, the efficiency of the boost converter and the grid-tie inverter increases with the increase of the period of the simulated wave and the efficiency of the system, from the input of mechanical energy to the production of electrical energy in the grid, stays almost constant with the increase of the period of the simulated wave.

Also, it is possible to see that the generator is the least efficient component of the system, with an efficiency in the simulated wave tests between $31.2\%$ and $48.4\%$.

# 4. Conclusion

In conclusion, in this project, an AC-DC-AC converter was developed to enable the connection of the generator to the electrical grid, destined for a WEC, with the use of the wind generator controller, a boost converter and a grid-tie inverter. In this way, the wind generator controller makes the AC-DC conversion, the boost converter raises the DC voltage to be able to keep the grid-tie inverter online when the generator is at low RPM and the grid-tie inverter does the DC-AC conversion.

This system allows the production of energy for the electrical network with the capture of energy from the waves of the sea, through the vertical movement of a buoy.

Since the prototype has not yet been built, it depends on future work to build it, so that later we can truly know the efficiency of the PTO developed and the extent of the objectives achieved.

With the tests and trials carried out, it was found that the least efficient component is the generator. This problem can be solved by replacing the generator with another type of generator, namely DFIG or Squirrel Cage Induction Generator (SCIG) generators, which are the types of generators that are currently used in real cases in electricity production plants.

A point of future improvement would be the addition of a flywheel before the generator in conjunction with the boost converter to smooth the recovered energy, allowing a more constant curve of the electricity produced.

Intentionally blank page.

# References

[1] "Electricity – World Energy Outlook 2019 – Analysis - IEA", https://www.iea.org/reports/world-energy-outlook-2019/electricity. (Accessed in 02/03/2022)

[2] The European Commission, "The European Green Deal", 2019.

[3] European Commission, "Energy roadmap 2050", Publications Office of the European Union, Luxembourg, 2012.

[4] Lanre Olatomiwa, Saad Mekhilef, M.S. Ismail and M. Moghavvemi, "Energy management strategies in hybrid renewable energy systems: A review", Renewable and Sustainable Energy Reviews, 62:821–835, 2016.

[5] Yimy E. García Vera, Rodolfo Dufo-López and José L. Bernal-Agustín, "Energy management in microgrids with renewable energy sources: A literature review", Applied Sciences, 9(18), 2019.

[6] P. Mccullen et al., "Wave energy in Europe: current status and perspectives", vol. 6, pp. 405–431, 2002.

[7] Daniela Valente, "Mecanismos inovadores para recuperação de energia do movimento do mar", Master's thesis, Universidade de Aveiro, Aveiro, 2019.

[8] Paulo Cardoso, "Desenvolvimento de sistema para recuperação de energia das ondas", Master's thesis, Universidade de Aveiro, Aveiro, 2021.

[9] O. M. Phillips, "The dynamics of the upper ocean", 2nd edition, Cambridge University Press, 1977.

[10] Ocean Energy Council, "Tidal Energy", 2008.

[11] J. N. Moore, S. F. Simmons, "More power from below", Science, 340 (6135), p. 933-934, 2013.

[12] Makai Ocean Engineering, "Ocean Thermal Energy Conversion", 2013.

[13] R. E. Pattle, "Production of electric power by mixing fresh and salt water in the hydroelectric pile", Nature, 174 (4431): 660, October 2nd 1954.

[14] Dominique Egré, Joseph Milewski, "The diversity of hydropower projects", Energy Policy, 30 (14): 1225–1230, 2002.

[15] S. Portland, "A Pelamis installed at the Agucadoura Wave Park off Portugal", July 2008.

[16] Kim Rutledge, Melissa McDaniel, Santani Teng, Hilary Hall, Tara Ramroop, Erin Sprout, Jeff Hunt, Diane Boudreau and Hilary Costa, "Tidal energy", National Geographic Society, May 20th 2022.

[17] Nozar Poursheikhian, "Geothermal Energy", Quchan University of Advanced Technologies Engineering, December 1st 2013.

[18] The Climate Technology Centre and Network, "Osmotic power", March 2011.

[19] Allen Watkin, "Three Gorges Dam", The Dam, September 2008.

[20] I. López, J. Andreu, S. Ceballos, I. Martínez De Alegría and I. Kortabarria, “Review of wave energy technologies and the necessary power-equipment”, Renew. Sustain. Energy Rev., vol. 27, pp. 413–434, 2013.

[21] Amelie Tetu, “Power Take-Off Systems for WECs”, pages 203–220, Springer, Cham, January 2017.

[22] R. Henderson, “Design, simulation and testing of a novel hydraulic power take-off system for the Pelamis wave energy converter”, vol. 31, pp. 271–283, 2006.

[23] I. S. A. A. Rodrigues and E. Eletrotécnica, “Estudo do Galgamento em Conversor de Ondas Oceânicas”, Instituto Superior de Engenharia de Lisboa, 2017.

[24] D. Roddier, C. Cermelli, A. Aubault and A. Weinstein, “WindFloat: A floating foundation for offshore wind turbines”, J. Renew. Sustain. Energy, vol. 2, no. 3, 2010.

[25] C. Josset and A. H. Clément, “A time-domain numerical simulator for oscillating water column wave power plants”, Renew. Energy, vol. 32, no. 8, pp. 1379–1402, 2007.

[26] A. F. d. O. Falcão, “Wave energy utilization: A review of the technologies”, Renew. Sustain. Energy Rev., vol. 14, no. 3, pp. 899–918, 2010.

[27] B. Wu, T. Chen, J. Jiang, G. Li, Y. Zhang and Y. Ye, “Economic assessment of wave power boat based on the performance of ‘Mighty Whale’ and BBDB”, Renew. Sustain. Energy Rev., vol. 81, no. May 2017, pp. 946–953, 2018.

[28] P. E. Ventures, “Oregon Wave Energy Trust Utility Market Initiative Task 2.1.2: Garrad Hassan Wave Energy Technology Review”, Energy, no. December, 2009.

[29] J. R. Joubert, J. L. Van Niekerk and J. Reinecke, “LIST Wave Energy Converters”, vol. 27, no. 0, pp. 0–95, 2013.

[30] L. Wang, J. Isberg and E. Tedeschi, “Review of control strategies for wave energy conversion systems and their validation: the wave-to-wire approach”, Renew. Sustain. Energy Rev., vol. 81, no. October 2016, pp. 366–379, 2018.

[31] T. Whittaker and M. Folley, “Nearshore oscillating wave surge converters and the development of Oyster”, Philos. Trans. R. Soc. A Math. Phys. Eng. Sci., vol. 370, no. 1959, pp. 345–364, 2012.

[32] A. Rafiee and J. Fiévez, “Numerical Prediction of Extreme Loads on the CETO Wave Energy Converter”, Proc. 11th Eur. Wave Tidal Energy Conf., no. December, 2015.

[33] J. D. Bricker, M. Esteban, H. Takagi and V. Roeber, “Economic feasibility of tidal stream and wave power in post-Fukushima Japan”, Renew. Energy, vol. 114, pp. 32–45, 2017.

[34] A. Pecher, J. P. Kofoed and T. Larsen, “Design specifications for the hanstholm WEPTOS wave energy converter”, Energies, vol. 5, no. 4, pp. 1001–1017, 2012.

[35] J. P. Kofoed, “Model Testing of the Wave Energy Converter Seawave Slot-Cone Generator”, Hydraul. Coast. Eng., vol. 18, 2005.

[36] C. Jones, J. Magalen and J. Roberts, “Wave Energy Converter (WEC) Array Effects on Wave, Current and Sediment Circulation: Monterey Bay, CA”, no. September, 2014.

[37] A. F. O. Falcão, J. J. Cândido, P. A. P. Justino and J. C. C. Henriques, “Hydrodynamics of the IPS buoy wave energy converter including the effect of non-uniform acceleration tube cross section”, Renew. Energy, vol. 41, pp. 105–114, 2012.

[38] A. Wacher, “Mathematical and Numerical Modeling of the AquaBuOY Wave Energy Converter”, Math. Case Stud., vol. 2, no. February, pp. 16–33, 2010.

[39] X. Garnaud and C. C. Mei, “Comparison of wave power extraction by a compact array of small buoys and by a large buoy”, IET Renew. Power Gener., vol. 4, no. 6, p. 519, 2010.

[40] E. Rusu and F. Onea, “Study on the influence of the distance to shore for a wave energy farm operating in the central part of the Portuguese nearshore”, ENERGY Convers. Manag., vol. 114, pp. 209–223, 2016.

[41] J. Weber, F. Mouwen, A. Parish and D. Robertson, “Wavebob – Research & Development Network and Tools in the Context of Systems Engineering”, Ewtec, no. Proc. of the 8th European Wave and Tidal Energy Conf., Uppsala, Sweden, pp. 416–420, 2009.

[42] R. H. Hansen, M. M. Kramer and E. Vidal, “Discrete displacement hydraulic power take-off system for the wavestar wave energy converter”, Energies, vol. 6, no. 8, pp. 4001–4044, 2013.

[43] A. Pecher, J. P. Kofoed and S., “Handbook of Ocean Wave Energy”, 2017.

[44] A. P. McCabe, A. Bradshaw, J. A. C. Meadowcroft and G. Aggidis, “Developments in the design of the PS Frog Mk 5 wave energy converter”, Renew. Energy, vol. 31, no. 2, pp. 141–151, 2006.

[45] C. Pérez-Collazo, D. Greaves, and G. Iglesias, “A review of combined wave and offshore wind energy”, Renew. Sustain. Energy Rev., vol. 42, pp. 141–153, 2015.

[46] G. Bracco, A. Cagninei, E. Giorcelli, G. Mattiazzo, D. Poggi and M. Raffero, “Experimental validation of the ISWEC wave to PTO model”, Ocean Eng., vol. 120, pp. 40–51, 2016.

[47] D. D. Grilo, “Geração de energia a partir das ondas do mar”, 2013.

[48] U. Azimov, “Feasibility study and design of an ocean wave power generation station integrated with a decommissioned offshore oil platform in UK waters”, vol. 8, pp. 161–174, 2017.

[49] Markel Penalba and John Ringwood, “A review of wave-to-wire models for wave energy converters”, Energies, 7:506, June 17th 2016.

[50] Max Erland, FPEC, “Free Piston Energy Converter”, EVS 21 Monaco, 2005.

[51] Omar Farrok, Koushik Ahmed, Abdirazak Dahir Tahlil, Mohamud Mohamed Farah, Mahbubur Rahman Kiran and Md. Rabiul Islam, “Electrical power generation from the oceanic wave for sustainable advancement in renewable energy technologies”, Sustainability, 12(6), 2020.

[52] G. J. Dalton, R. Alcorn, and T. Lewis, “Case study feasibility analysis of the Pelamis wave energy convertor in Ireland, Portugal and North America”, Renew. Energy, vol. 35, no. 2, pp. 443–455, 2010.

[53] André F. R. de Sá and António E. P. C. Barbosa, “Máquinas Elétricas e Alguns Engenhos - 2.ª Edição”, Porto, 2017.

[54] G. Marques and M. J. Resende, “Máquinas de Indução Polifásicas”, Curso de Máquinas Eléctricas, Universidade Técnica de Lisboa: Instituto Superior Técnico, 2007.

[55] R. Gagnon et al., “Modeling and Real-Time Simulation of a Doubly-Fed Induction Generator Driven by a Wind Turbine”, Montreal, Canada: International Conference on Power Systems Transients, 2005.

[56] Bram Van Eeckhout, “The economic value of VSC HVDC compared to HVAC for offshore wind farms”, Master’s thesis, Elektrotechniek Dept., Katholieke Universiteit Leuven, Heverlee, Belgium, 2008.

[57] “Yuzo Wind Turbine”, https://www.tesup.co.uk/product-page/yuzo-wind-turbine-made-in-europe. (Accessed in 05/02/2022)

[58] “Wind Turbine Charge Controller”, https://www.tesup.co.uk/product-page/buy-12v-24v-48v-wind-charge-controller-uk. (Accessed in 05/02/2022)

[59] D. John Pradeep, Mathew Mithra Noel and N. Arun, “Nonlinear control of a boost converter using a robust regression based reinforcement learning algorithm”, Engineering Applications of Artificial Intelligence., 52: 1–9, June 1st 2016.

[60] Alexandre Manuel M. N. da Mota, “Electrónica de Potência”, DETI-UA, Aveiro, October 2nd 2020.

[61] Kevin C. Fronczak, “Comparison of Optimization Algorithms for Boost Converter Controller Design”, Department of Electrical and Microelectronic Engineering, Rochester Institute of Technology, August 2013.

[62] Luiz Carlos, “Inversores de Freqüência”, Universidade Federal de Santa Maria, November 4th 2013.

[63] Jim Doucet, Dan Eggleston and Jeremy Shaw, “DC/AC Pure Sine Wave Inverter”, Worcester Polytechnic Institute, 2006-2007.

[64] “Microinversor 250W/20-50V”, https://4sat.pt/product/microinversor-250w20-50v-ligacao-a-rede-gen1. (Accessed in 18/08/2022)

[65] “Brochure onduleurs IEnergy”, http://www.neo-energy.eu/download/Brochure%20onduleurs%20IEnergy.pdf. (Accessed in 18/08/2022)

[66] “Fully Integrated, Hall Effect-Based Linear Current Sensor with 2.1 kVRMS Voltage Isolation and a Low-Resistance Current Conductor”, https://www.sparkfun.com/datasheets/BreakoutBoards/0712.pdf. (Accessed in 19/08/2022)

[67] “ZMPT101B Current-type Voltage Transformer”, https://5krorwxhmqqirik.leadongcdn.com/ZMPT101B+specification-aidijBqoKomRilSqqokpjkp.pdf. (Accessed in 19/08/2022)

[68] “FR-S500 Instruction Manual (Basic)”, https://dl.mitsubishielectric.com/dl/fa/document/manual/inv/ib0600026/ib0600026d.pdf. (Accessed in 20/05/2022)

[69] Pedro N. F. da Fonseca, “Sistemas de Instrumentação Electrónica”, DETI-UA, Aveiro, 2020/21.

[70] ENERGY STAR Canada, “Application considerations and estimated Savings for VFD Drives”, ENERGY STAR announcements publications, Canada, December 17th 2015.

[71] Mubarak Shah et al., “Efficiency Evaluation of Three Phase and Single Phase C2C Self-Excited Induction Generator for Micro Hydro Power Application”, School of Renewable Energy Technology, Naresuan University Phitsanulok 65000, Thailand, 2017.

[72] “AC Circuit Loads”, Pumps & Systems, August 2010.

Intentionally blank page.

# Appendix A

# 2D drawings of the structure

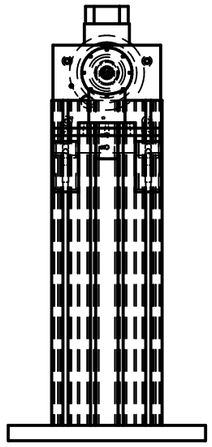

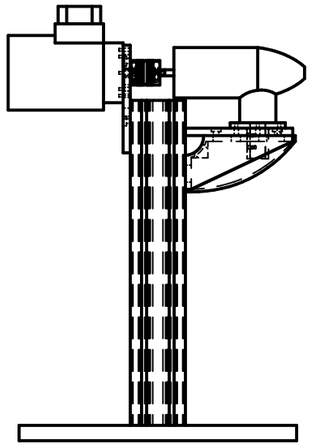

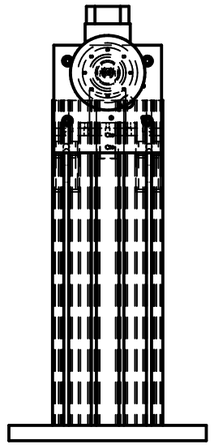

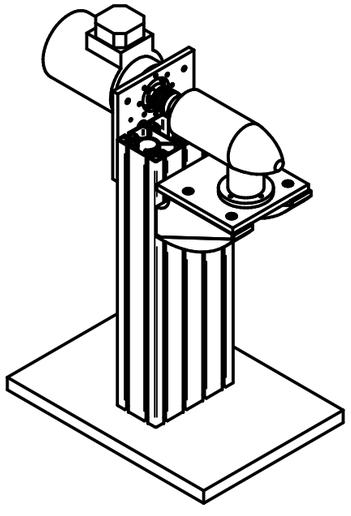

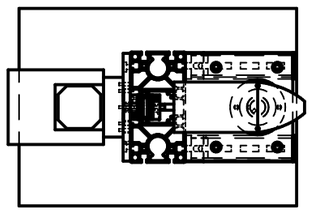

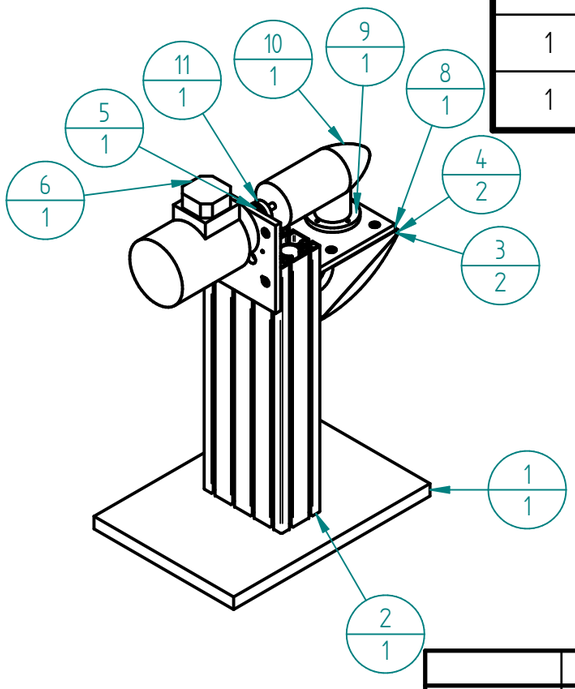


REVISION HISTORY

| REV | DESCRIPTION | DATE | APPROVED |
|---|---|---|---|
| | | | |

| Quantity | File Name (no extension) | Document Number | Material | Item Number |
|---|---|---|---|---|
| 1 | Base_V2 | | | 1 |
| 1 | 20_1013_0_2 | | | 2 |
| 2 | Plate_Support_V2 | | | 3 |
| 2 | Plate_Support_Cover_V2 | | | 4 |
| 1 | Motor_Support_V3 | | | 5 |
| 1 | Motor_Dummy | | | 6 |
| 1 | Motor_Shaft_Bushing | | Al 5xxx | 7* |
| 1 | Generator_Plate_V3 | | Al 5xxx | 8 |
| 1 | suporte gerador v3 | | Al 5xxx | 9 |
| 1 | Generator_Dummy | | | 10 |
| 1 | Acoplador | | | 11 |

| | NAME | DATE |
|---|---|---|
| DRAWN | Daniel Gadelha | 03/30/22 |
| CHECKED | | |
| ENG APPR | | |
| MGR APPR | | |

FINISH ISO 2768-mk ISO 8015

NOTES UNLESS OTHERWISE SPECIFIED DIMENSIONS ARE IN MILLIMETERS ANGLES ±X.X° 2 PL ±X.XX 3 PL ±X.XXX

Solid Edge

TITLE Overview

MATERIAL

SIZE A3 | DWG NO | REV

FILE NAME: Draft_V3.dft

SCALE: | WEIGHT: | SHEET 1 OF 4

| REVISION HISTORY | | | |
|---|---|---|---|
| REV | DESCRIPTION | DATE | APPROVED |
| | | | |

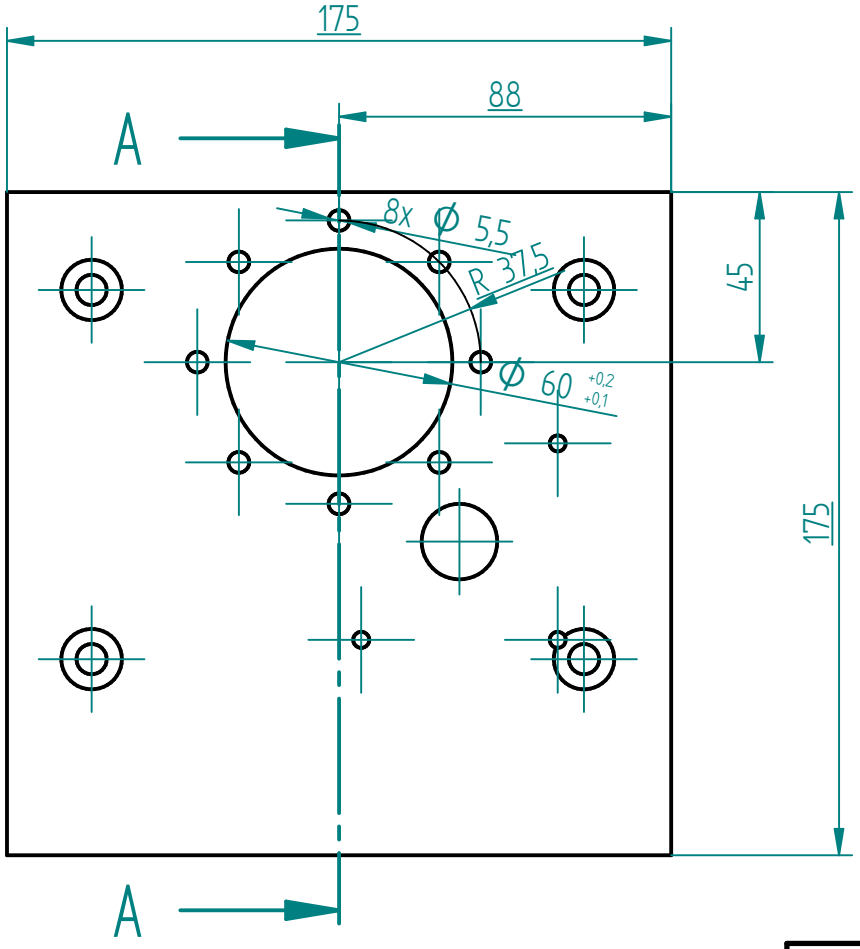


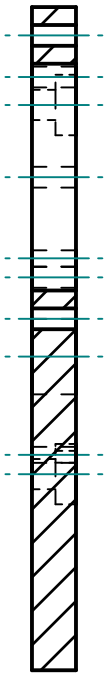

SECTION A–A

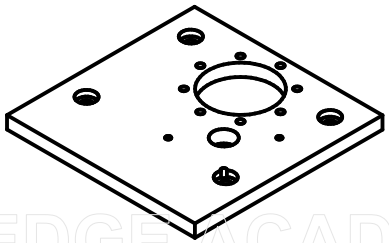

| | NAME | DATE |
|---|---|---|
| DRAWN | Daniel Gadelha | 03/30/22 |
| CHECKED | | |
| ENG APPR | | |
| MGR APPR | | |

| | |
|---|---|
| FINISH | ISO 2768-mk<br>ISO 8015 |
| NOTES | UNLESS OTHERWISE SPECIFIED<br>DIMENSIONS ARE IN MILLIMETERS<br>ANGLES ±X.X°<br>2 PL ±X.XX 3 PL ±X.XXX |

Solid Edge

| | |
|---|---|
| TITLE | Motor Support |
| MATERIAL | Al 5xxx |
| SIZE | A4 |
| DWG NO | |
| REV | |
| FILE NAME: | Draft_V3.dft |
| SCALE: | |
| WEIGHT: | |
| SHEET 2 OF 4 | |

| REVISION HISTORY | | | |
|---|---|---|---|
| REV | DESCRIPTION | DATE | APPROVED |
| | | | |

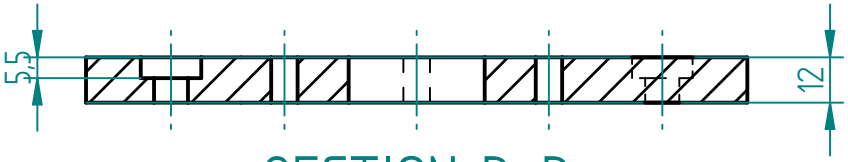


SECTION B–B

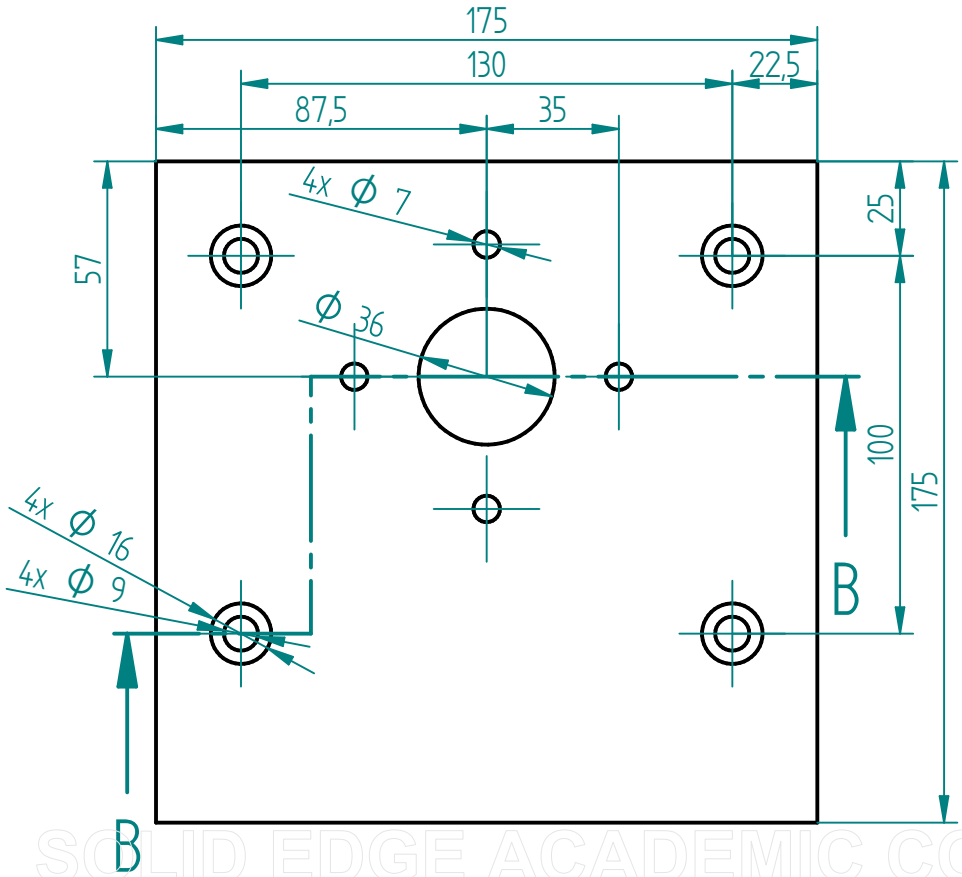


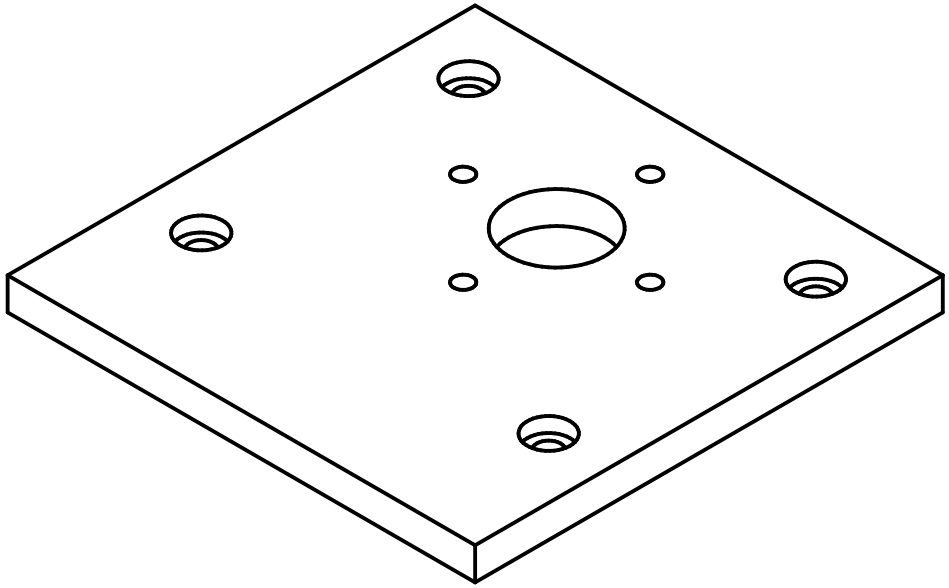

| | NAME | DATE |
|---|---|---|
| DRAWN | Daniel Gadelha | 03/30/22 |
| CHECKED | | |
| ENG APPR | | |
| MGR APPR | | |

FINISH: ISO 2768-mk, ISO 8015

NOTES: UNLESS OTHERWISE SPECIFIED DIMENSIONS ARE IN MILLIMETERS ANGLES ±X.X° 2 PL ±X.XX 3 PL ±X.XXX

Solid Edge

TITLE: Generator Plate

MATERIAL: Al 5xxx

SIZE: A4 | DWG NO | REV

FILE NAME: Draft_V3.dft

SCALE: | WEIGHT: | SHEET 3 OF 4

| REVISION HISTORY | | | |
|---|---|---|---|
| REV | DESCRIPTION | DATE | APPROVED |
| | | | |

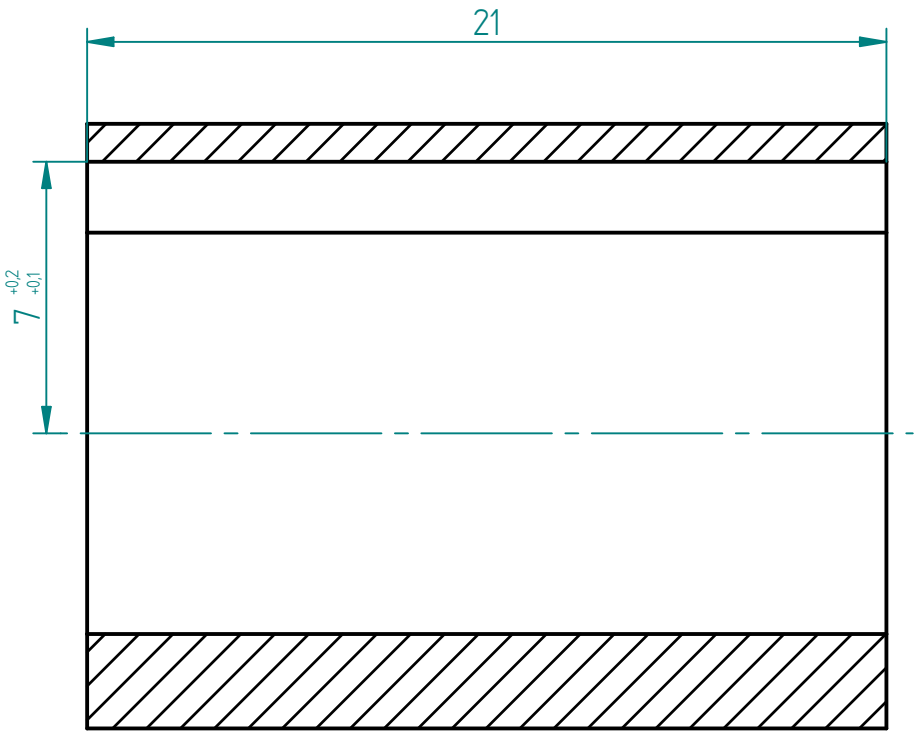


SECTION C-C

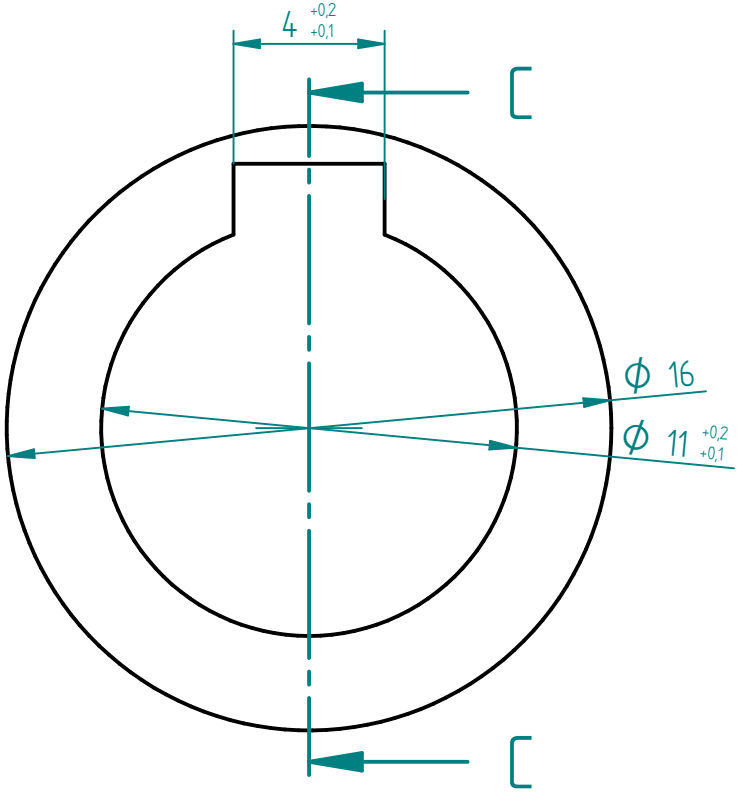


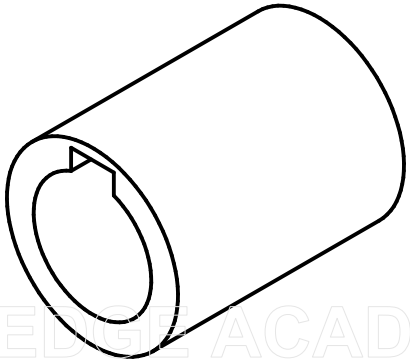

| | NAME | DATE |
|---|---|---|
| DRAWN | Daniel Gadelha | 03/30/22 |
| CHECKED | | |
| ENG APPR | | |
| MGR APPR | | |

FINISH: ISO 2768-mk, ISO 8015

NOTES: UNLESS OTHERWISE SPECIFIED
DIMENSIONS ARE IN MILLIMETERS
ANGLES ±X.X°
2 PL ±X.XX 3 PL ±X.XXX

Solid Edge

TITLE: Motor Shaft Bushing

MATERIAL: Al 5xxx

| SIZE | DWG NO | REV |
|---|---|---|
| A4 | | |

FILE NAME: Draft_V3.dft

| SCALE: | WEIGHT: | SHEET 4 OF 4 |
|---|---|---|

| REVISION HISTORY | | | |
|---|---|---|---|
| REV | DESCRIPTION | DATE | APPROVED |
| | | | |

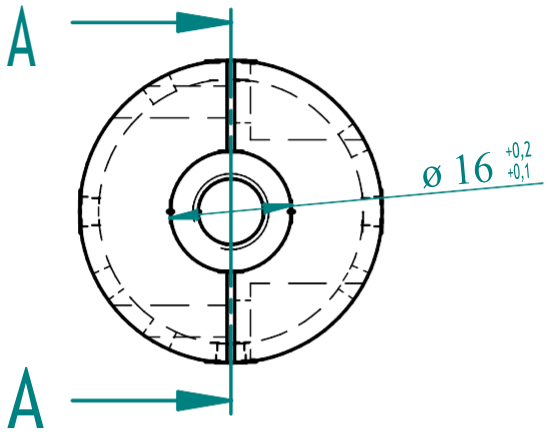


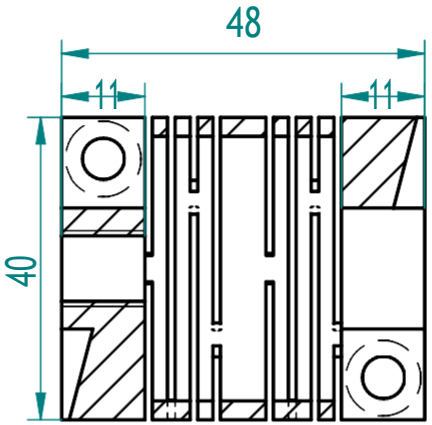


SECTION A-A

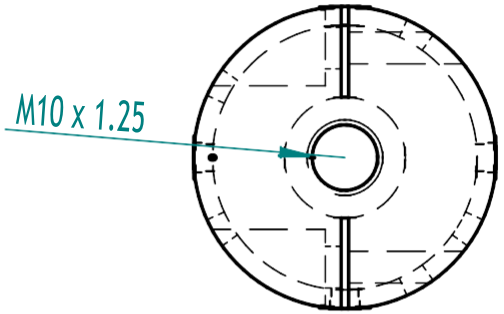


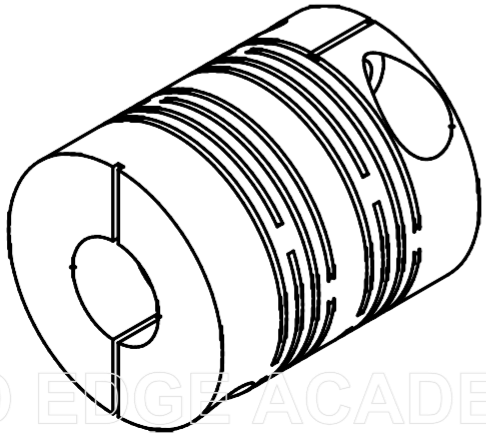

| | NAME | DATE |
|---|---|---|
| DRAWN | Daniel Gadelho | 03/30/22 |
| CHECKED | | |
| ENG APPR | | |
| MGR APPR | | |

FINISH ISO 2768-mk ISO 8015

NOTES UNLESS OTHERWISE SPECIFIED DIMENSIONS ARE IN MILLIMETERS ANGLES ±X.X° 2 PL ±X.XX 3 PL ±X.XXX

**Solid Edge**

TITLE Coupling

MATERIAL Al 5xxx

SIZE A4 | DWG NO | REV

FILE NAME: Draft_V4.dft

SCALE: | WEIGHT: | SHEET 5 OF 5

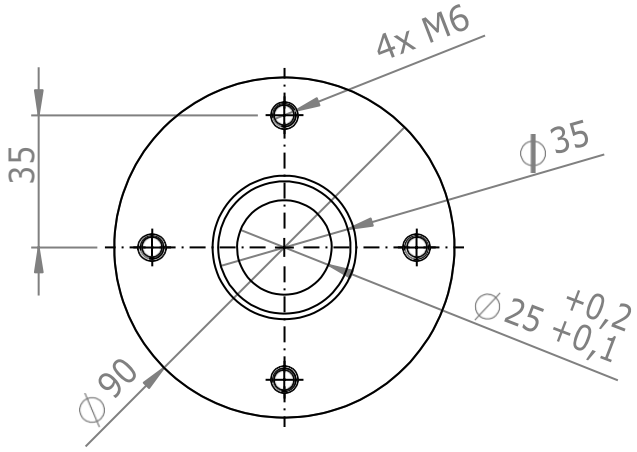


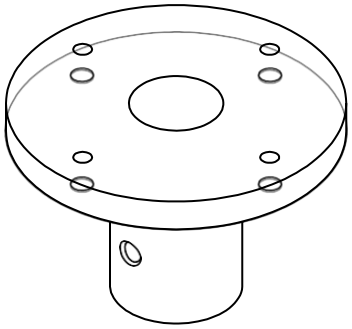

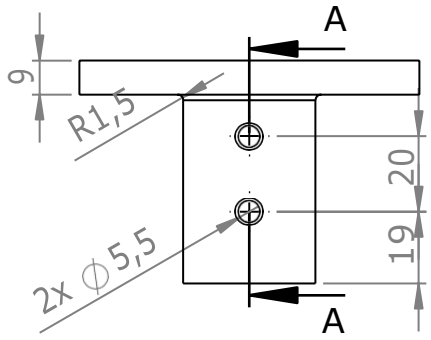


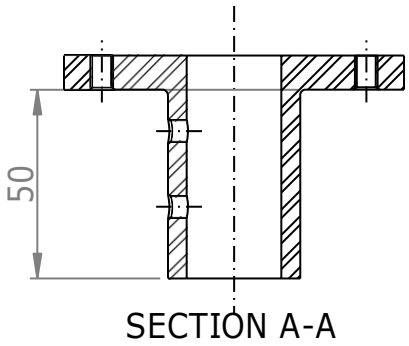


SECTION A-A

| | | | |
|---|---|---|---|
| UNLESS OTHERWISE SPECIFIED:<br>DIMENSIONS ARE IN MILLIMETERS<br>SURFACE FINISH:<br>TOLERANCES:<br>LINEAR:<br>ANGULAR: | FINISH: ISO 2768-mk<br>ISO 8015 | DEBURR AND BREAK SHARP EDGES | DO NOT SCALE DRAWING | REVISION |

| | NAME | SIGNATURE | DATE |
|---|---|---|---|
| DRAWN | Gonçalo Pires | | |
| CHK'D | | | |
| APPV'D | | | |
| MFG | | | |
| Q.A | | | |

TITLE:

MATERIAL: Al 5xxx

DWG NO. suporte gerador v3

A4

WEIGHT:

SCALE:1:2

SHEET 1 OF 1

Intentionally blank page.

# Appendix B

# Electrical diagram

Tel.

| | |
|---|---|
| Empresa / Cliente | |
| Descrição do projeto | Desenvolvimento de protótipo para recuperação de energia das ondas |
| Número de projeto | |
| Comissão | |

| | |
|---|---|
| Fabricante (Empresa) | |
| Coluna | |
| Nome do projeto | Desenvolvimento de protótipo para recuperação de energia das ondas |
| Realizar | |
| Tipo | |
| Localização de instalação | |
| Responsável pelo projeto | |
| Características da peça | |

| | | | |
|---|---|---|---|
| Criado em | 26/03/2021 | | |
| Editado em | 11/12/2022 | de (abreviatura) EPLAN | Quantidade de páginas 5 |

# Tabela de conteúdos

Coluna X: uma página gerada automaticamente foi alterada manualmente

F06_001

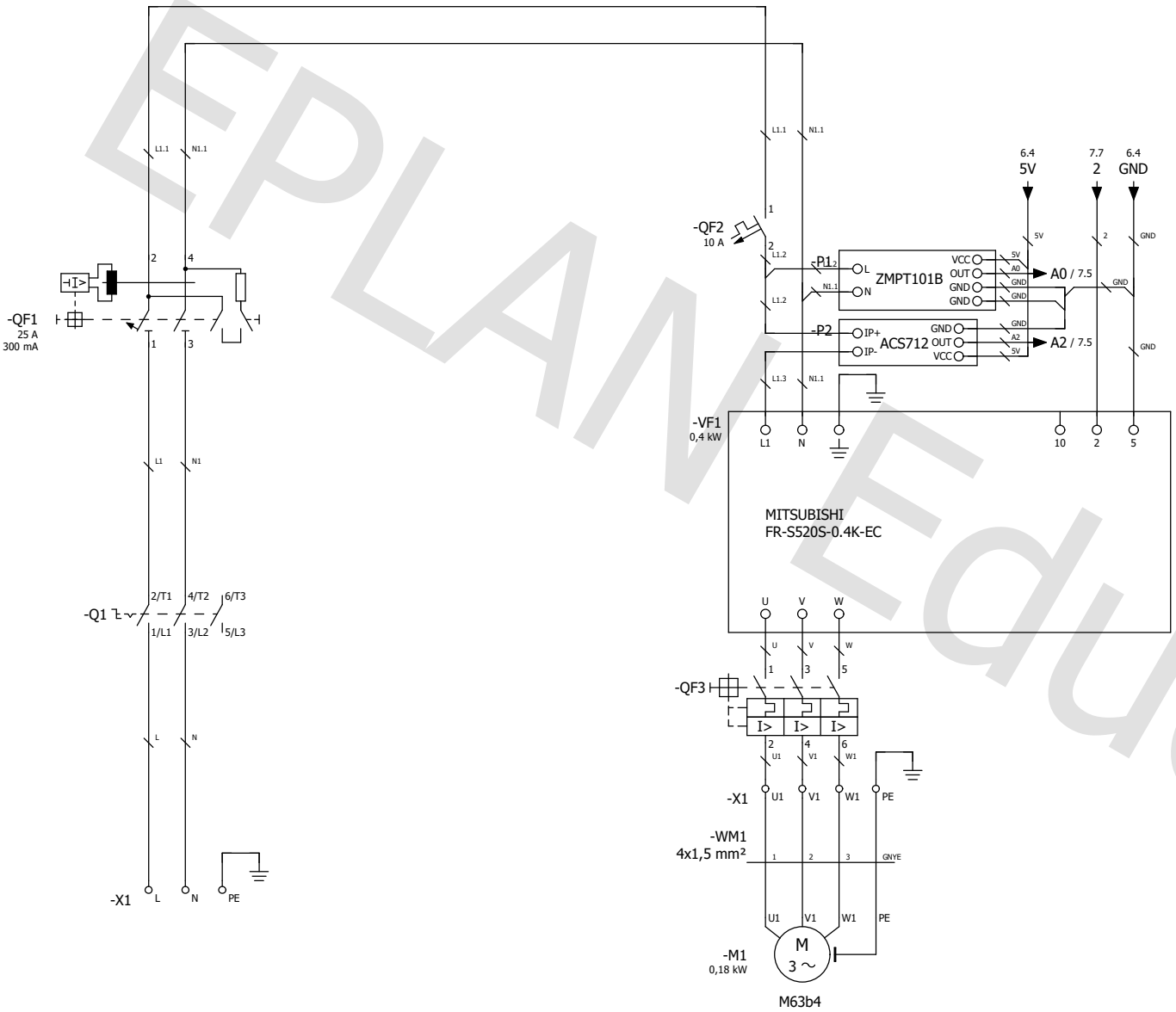




2 6

| | | | | | | | | | |
|---|---|---|---|---|---|---|---|---|---|
| | | | Data | 11/12/2022 | | | Potência | | = |
| | | | Editor. | EPLAN | | | | | + |
| | | | Verif | | Desenvolvimento de protótipo para recuperação de energia das ondas | | | | Folha 5 |
| Alteração | Data | Nome | Orig | | Em substituição de | Substituído por | | | Página 3 / 5 |

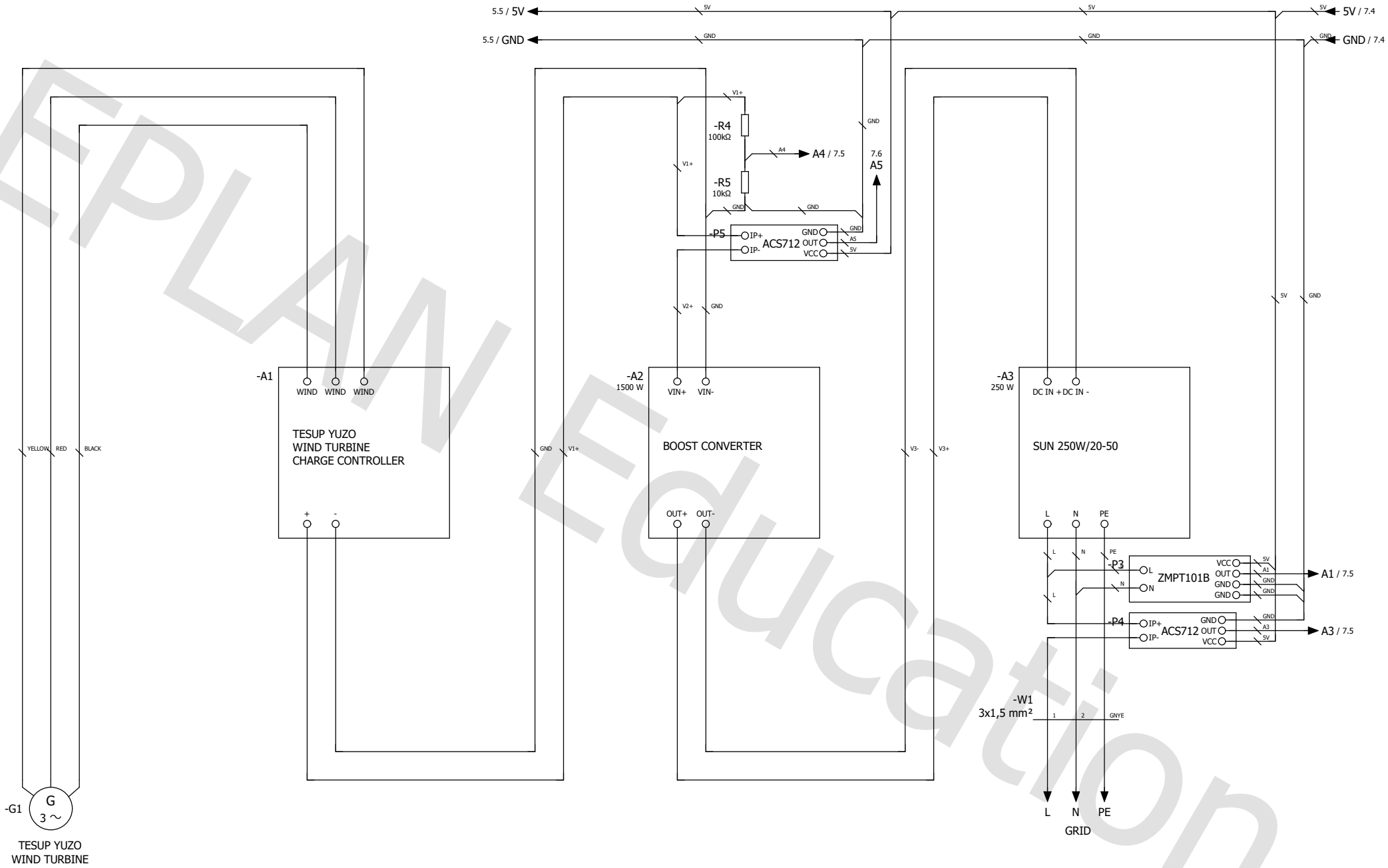




| | | | | | | | | | |
|---|---|---|---|---|---|---|---|---|---|
| | | | Data | 11/12/2022 | | | Potência | | = |
| | | | Editor. | EPLAN | | | | | + |
| | | | Verif | | Desenvolvimento de protótipo para recuperação de energia das ondas | | | | Folha 6 |
| Alteração | Data | Nome | Orig | | Em substituição de | Substituído por | | | Página 4 / 5 |

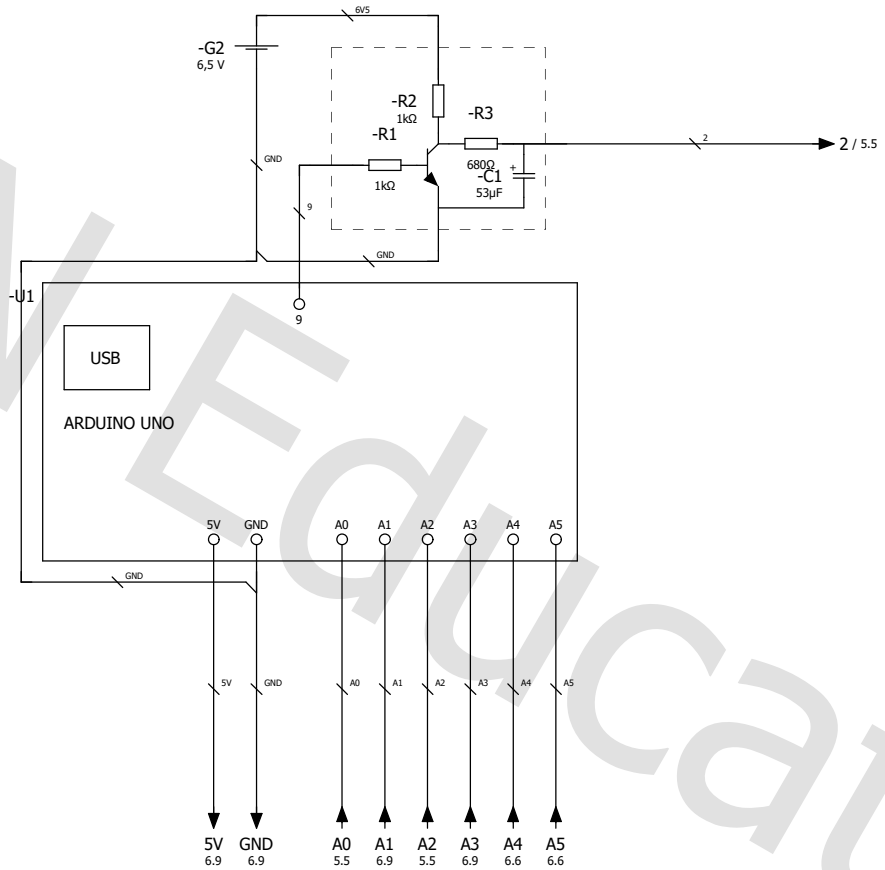




6

| | | | | | | | | | |
|---|---|---|---|---|---|---|---|---|---|
| | | | Data | 11/12/2022 | | | Sinais digitais e analógicos | | = |
| | | | Editor. | EPLAN | | | | | + |
| | | | Verif | | Desenvolvimento de protótipo para recuperação de energia das ondas | | | | Folha 7 |
| Alteração | Data | Nome | Orig | | Em substituição de | Substituído por | | | Página 5 / 5 |

# Appendix C

# Arduino code

```
// AC Energy Meter and Electric Motor Control via VFD
// Based on AC Energy Meter with LCD by Solarduino

int motorPin = 9;    // the PWM pin
int motorValue = 0;
int motorValueAmount = 5;
float motorLastSample = 0;

int VoltageAnalogInputPin_1 = A0;
float voltageSampleRead_1 = 0;
float voltageLastSample_1 = 0;
float voltageSampleSum_1 = 0;
float voltageSampleCount_1 = 0;
float voltageMean_1;
float RMSVoltageMean_1;

float voltageOffset1_1 = 0;
float voltageOffset2_1 = 0;

int VoltageAnalogInputPin_2 = A1;
float voltageSampleRead_2 = 0;
float voltageLastSample_2 = 0;
float voltageSampleSum_2 = 0;
float voltageSampleCount_2 = 0;
float voltageMean_2;
float RMSVoltageMean_2;

float voltageOffset1_2 = 0;
float voltageOffset2_2 = 0;

int CurrentAnalogInputPin_1 = A2;
float mVperAmpValue_1 = 66;

float currentSampleRead_1 = 0;
float currentLastSample_1 = 0;
float currentSampleSum_1 = 0;
float currentSampleCount_1 = 0;
float currentMean_1;
float RMSCurrentMean_1 = 0;
float FinalRMSCurrent_1;

float currentOffset1_1 = 0;
float currentOffset2_1 = 0;

int CurrentAnalogInputPin_2 = A3;
float mVperAmpValue_2 = 66;

float currentSampleRead_2 = 0;
float currentLastSample_2 = 0;
float currentSampleSum_2 = 0;
float currentSampleCount_2 = 0;
float currentMean_2;
float RMSCurrentMean_2 = 0;
float FinalRMSCurrent_2;

float currentOffset1_2 = 0;
float currentOffset2_2 = 0;

int VoltageAnalogInputPin_3 = A4;
float voltageSampleRead_3 = 0;

int CurrentAnalogInputPin_3 = A5;
float mVperAmpValue_3 = 185;

float currentOffset1_3 = 0;

float sampleCurrent1_1;
float sampleCurrent2_1;
float sampleCurrent3_1;
float apparentPower_1;
float realPower_1 = 0;
float powerSampleRead_1 = 0;
float powerLastSample_1 = 0;
float powerSampleCount_1 = 0;
float powerSampleSum_1 = 0;
float powerFactor_1 = 0;

float powerOffset_1 = 0;

float sampleCurrent1_2;
float sampleCurrent2_2;
float sampleCurrent3_2;
float apparentPower_2;
float realPower_2 = 0;
float powerSampleRead_2 = 0;
float powerLastSample_2 = 0;
float powerSampleCount_2 = 0;
float powerSampleSum_2 = 0;
float powerFactor_2 = 0;

float powerOffset_2 = 0;

float realPower_3 = 0;
float powerLastSample_3 = 0;



void setup()
{
    Serial.begin(9600);

    pinMode(motorPin, OUTPUT);
}
```

```
void loop()
{
    // Motor Control
    if(millis() >= motorLastSample + 30)            // taking 1 action every 30 ms, 7 ms for waves of 0.5 s of period,
    {                                               //                              13 ms for waves of 1 s of period,
        analogWrite(motorPin, motorValue);          //                              26 ms for waves of 2 s of period,
        motorValue = motorValue + motorValueAmount; //                              39 ms for waves of 3 s of period,
        if(motorValue <= 0 || motorValue >= 190)    //                              53 ms for waves of 4 s of period,
        {                                           //                              66 ms for waves of 5 s of period
            motorValueAmount = -motorValueAmount;
        }
        motorLastSample = millis();
    }

    // AC Voltage Measurement of A0
    if(millis() >= voltageLastSample_1 + 1) // taking 1 reading every 1 ms
    {
        voltageSampleRead_1 = 2 * (analogRead(VoltageAnalogInputPin_1) - 512) + voltageOffset1_1;
        voltageSampleSum_1 = voltageSampleSum_1 + sq(voltageSampleRead_1);
        voltageSampleCount_1 = voltageSampleCount_1 + 1;
        voltageLastSample_1 = millis();
    }

    if(voltageSampleCount_1 == 20) // after 20 counts, that is, after 20 ms, which is 50 Hz
    {
        voltageMean_1 = voltageSampleSum_1 / voltageSampleCount_1;
        RMSVoltageMean_1 = sqrt(voltageMean_1) + voltageOffset2_1;
        Serial.print("V1 = ");
        Serial.print(RMSVoltageMean_1, 1);
        Serial.print(" V   ");
        voltageSampleSum_1 = 0;
        voltageSampleCount_1 = 0;
    }

    // AC Voltage Measurement of A1
    if(millis() >= voltageLastSample_2 + 1) // taking 1 reading every 1 ms
    {
        voltageSampleRead_2 = 2 * (analogRead(VoltageAnalogInputPin_2) - 512) + voltageOffset1_2;
        voltageSampleSum_2 = voltageSampleSum_2 + sq(voltageSampleRead_2);
        voltageSampleCount_2 = voltageSampleCount_2 + 1;
        voltageLastSample_2 = millis();
    }

    if(voltageSampleCount_2 == 20) // after 20 counts, that is, after 20 ms, which is 50 Hz
    {
        voltageMean_2 = voltageSampleSum_2 / voltageSampleCount_2;
        RMSVoltageMean_2 = sqrt(voltageMean_2) + voltageOffset2_2;
        Serial.print("V2 = ");
        Serial.print(RMSVoltageMean_2, 1);
        Serial.print(" V   ");
        voltageSampleSum_2 = 0;
        voltageSampleCount_2 = 0;
    }

    // AC Current Measurement of A2
    if(millis() >= currentLastSample_1 + 1) // taking 1 reading every 1 ms
    {
        currentSampleRead_1 = analogRead(CurrentAnalogInputPin_1) - 512 + currentOffset1_1;
        currentSampleSum_1 = currentSampleSum_1 + sq(currentSampleRead_1);
        currentSampleCount_1 = currentSampleCount_1 + 1;
        currentLastSample_1 = millis();
    }

    if(currentSampleCount_1 == 20) // after 20 counts, that is, after 20 ms, which is 50 Hz
    {
        currentMean_1 = currentSampleSum_1 / currentSampleCount_1;
        RMSCurrentMean_1 = sqrt(currentMean_1) + currentOffset2_1;
        FinalRMSCurrent_1 = (((RMSCurrentMean_1 / 1024) * 5000) / mVperAmpValue_1);
        Serial.print("I1 = ");
        Serial.print(FinalRMSCurrent_1, 1 * 2);
        Serial.print(" A   ");
        currentSampleSum_1 = 0;
        currentSampleCount_1 = 0;
    }

    // AC Current Measurement of A3
    if(millis() >= currentLastSample_2 + 1) // taking 1 reading every 1 ms
    {
        currentSampleRead_2 = analogRead(CurrentAnalogInputPin_2) - 512 + currentOffset1_2;
        currentSampleSum_2 = currentSampleSum_2 + sq(currentSampleRead_2);
        currentSampleCount_2 = currentSampleCount_2 + 1;
        currentLastSample_2 = millis();
    }

    if(currentSampleCount_2 == 20) // after 20 counts, that is, after 20 ms, which is 50 Hz
    {
        currentMean_2 = currentSampleSum_2 / currentSampleCount_2;
        RMSCurrentMean_2 = sqrt(currentMean_2) + currentOffset2_2;
        FinalRMSCurrent_2 = (((RMSCurrentMean_2 / 1024) * 5000) / mVperAmpValue_2);
        Serial.print("I2 = ");
        Serial.print(FinalRMSCurrent_2, 1 * 2);
        Serial.print(" A   ");
        currentSampleSum_2 = 0;
        currentSampleCount_2 = 0;
    }

    // AC Power of A0 and A2
    if(millis() >= powerLastSample_1 + 1) // taking 1 reading every 1 ms
    {
        sampleCurrent1_1 = analogRead(CurrentAnalogInputPin_1) - 512 + currentOffset1_1;
```

```
        sampleCurrent2_1 = (sampleCurrent1_1 / 1024) * 5000;
        sampleCurrent3_1 = sampleCurrent2_1 / mVperAmpValue_1;
        voltageSampleRead_1 = 2 * (analogRead(VoltageAnalogInputPin_1) - 512) + voltageOffset1_1;
        powerSampleRead_1 = voltageSampleRead_1 * sampleCurrent3_1;
        powerSampleSum_1 = powerSampleSum_1 + powerSampleRead_1;
        powerSampleCount_1 = powerSampleCount_1 + 1;
        powerLastSample_1 = millis();
    }

    if(powerSampleCount_1 == 20) // after 20 counts, that is, after 20 ms, which is 50 Hz
    {
        realPower_1 = ((powerSampleSum_1 / powerSampleCount_1) + powerOffset_1);
        Serial.print("P1 = ");
        Serial.print(realPower_1, 1);
        Serial.print(" W   ");
        powerSampleSum_1 = 0;
        powerSampleCount_1 = 0;
    }

    // AC Power of A1 and A3
    if(millis() >= powerLastSample_2 + 1) // taking 1 reading every 1 ms
    {
        sampleCurrent1_2 = analogRead(CurrentAnalogInputPin_2) - 512 + currentOffset1_2;
        sampleCurrent2_2 = (sampleCurrent1_2 / 1024) * 5000;
        sampleCurrent3_2 = sampleCurrent2_2 / mVperAmpValue_2;
        voltageSampleRead_2 = 2 * (analogRead(VoltageAnalogInputPin_2) - 512) + voltageOffset1_2;
        powerSampleRead_2 = voltageSampleRead_2 * sampleCurrent3_2;
        powerSampleSum_2 = powerSampleSum_2 + powerSampleRead_2;
        powerSampleCount_2 = powerSampleCount_2 + 1;
        powerLastSample_2 = millis();
    }

    if(powerSampleCount_2 == 20) // after 20 counts, that is, after 20 ms, which is 50 Hz
    {
        realPower_2 = ((powerSampleSum_2 / powerSampleCount_2) + powerOffset_2);
        Serial.print("P2 = ");
        Serial.print(realPower_2, 1);
        Serial.print(" W   ");
        powerSampleSum_2 = 0;
        powerSampleCount_2 = 0;
    }

    // DC Measurement
    if(millis() >= powerLastSample_3 + 20) // taking 1 reading every 20 ms
    {
        voltageSampleRead_3 = analogRead(VoltageAnalogInputPin_3) * 55 / 1023;
        Serial.print("V3 = ");
        Serial.print(voltageSampleRead_3, 1);
        Serial.print(" V   ");
        currentSampleRead_3 = analogRead(CurrentAnalogInputPin_3) - 512 + currentOffset1_3;
        Serial.print("I3 = ");
        Serial.print(currentSampleRead_3, 1 * 2);
        Serial.print(" A   ");
        realPower_3 = voltageSampleRead_3 * currentSampleRead_3;
        Serial.print("P3 = ");
        Serial.print(realPower_3, 1);
        Serial.print(" W   ");
        powerLastSample_3 = millis();
    }
}
```